Modelling Water Temperature Evolution Under Partial Ice Cover

by

Erika Kember

A thesis
presented to the University of Waterloo
in fulfillment of the
thesis requirement for the degree of
Master of Mathematics
in
Applied Mathematics

Waterloo, Ontario, Canada, 2026

© Erika Kember 2026

Author's Declaration

I hereby declare that I am the sole author of this thesis. This is a true copy of the thesis, including any required final revisions, as accepted by my examiners.

I understand that my thesis may be made electronically available to the public.

Abstract

Water's nonlinear density as a function of temperature is an important factor in the overall state of a lake, and is one that frequently causes vertical mixing from density differences in the water column of freshwater lakes in cold climate zones during spring and fall. Horizontal mixing due to lateral density differences in said lakes is also possible, but is often not considered in lake temperature models. As climate change influences global temperatures and weather patterns, partial ice cover has become more prevalent on northern lakes during the winter. Due to the differing absorptive properties of ice and water, areas of a lake that are covered by ice can experience less radiative heating than areas of open water, causing the adjacent zones of water to have different densities and therefore driving horizontal transport between them. Currently the predominant lake temperature models are not well equipped to handle this type of horizontal transport that occurs under partial ice cover. This thesis presents a "simplest possible" differential equation box model for lake temperature under partial ice cover that incorporates horizontal transport between areas of open water and ice cover. It is evaluated on its ability to give realistic water temperature results. Two regimes are studied: first, a constant insolation framework for analysis of heat transport parameter values, and second is a day cycle framework in which an emissivity switch is implemented to increase physical realism.

Acknowledgements

There are many who I'd like to acknowledge for helping me in both my master's journey and the completion of this thesis. Firstly I must thank my supervisor, Marek Stastna, endlessly for being the most supportive mentor I could have asked for. His guidance has made me a better, more confident researcher. I am eternally grateful to have been taken on as his student. I am also grateful to my committee members, Francis Poulin and Barbara Zemskova, for taking the time to review this thesis and give me valuable feedback. As well, I owe my gratitude to my lab mates Leonard Korreshi, Chichi Zhou, and Khush Bhavsar, for being available for mathematical discussions and Python help while also making our lab space feel like home. To my lab "cousins", Jakob Braga and Rosalie Cormier, I am also so grateful for their coding help and friendly support. To my friends, Juliette Sinnot and Liz Yackoboski, thank you for making even the UW campus seem beautiful. To the countless other friends, acquaintances, and colleagues who have supported me to this point, thank you for offering your time, expertise, and patience.

I also must acknowledge my partner, Xander, who has supported and encouraged me throughout this endeavor. His support has been essential for me to take on and finish this challenge. As well, I am grateful to my sister Michaela, whose own master's experience allowed her to guide me through the difficult parts of graduate school. And I am grateful to Hannah, for always reminding me who I am outside of academics.

Lastly, I owe immense thanks to my parents, Guy and Sue. Their decision to homeschool has afforded me choices that I would never have otherwise had. Every milestone I reach, will be reached because of their determination and effort.

Dedication

To my first teacher, Dad.

Table of Contents

Author's Declaration ii

Abstract iii

Acknowledgements iv

Dedication v

List of Figures ix

List of Tables xii

1 Introduction 1

1.1 Climate Change Impacts to Seasonal Cycling of Ice Cover 1

1.1.1 Ice Cover Trends and Implications 1

1.1.2 Radiatively Driven Exchange 7

1.2 Existing Models 10
1.2.1 FLake 10
1.2.2 CLIMo 11
1.3 Box Models 12
1.4 Model Description and Goal 13
1.5 Thesis Outline 14

2 Technical Background and Model Derivation **15**

2.1 Radiation 15
2.1.1 Incoming Radiation 16
2.1.2 Outgoing Radiation 19
2.2 Transport 20
2.3 Building the Model 22
2.3.1 Derivation 22
2.3.2 Simplification 27

3 Results and Discussion **31**

3.1 Constant Insolation Framework 33
3.1.1 Model Without Transport 34
3.1.2 Linear Transport 35

3.1.3 Nonlinear Transport 39
3.1.4 Constant Insolation Framework Discussion 41
3.2 Constant Insolation With Box Length Inequality 43
3.2.1 Unequal Box Length Discussion 47
3.3 Day-Night Cycle 47
3.3.1 Day–Night Cycle Without Emissivity Switch 48
3.3.2 Day–Night cycle With Emissivity Switch 50
3.3.3 Day-Night Cycle Discussion 51

4 Conclusions and Future Work **54**

References **58**

APPENDIX **63**

A **64**

List of Figures

1.1 A pond near University of Waterloo Health Services under varying stages of ice cover. Pictures were taken during January - March 2025. 3

1.2 Plot of water's equation of state. Temperature of maximum density is marked and the cold water regime is highlighted in blue. 8

1.3 Schematic of the results found in Allum et al. [2]. The schematic shows a side view of the mixing that takes place between areas of low and high insolation absorption. Figure is taken from [2]. 9

1.4 From Duguay et al.[8], a schematic of the various surface fluxes considered in CLIMo. 12

2.1 A diagram depicting the absorptive behaviours of water and ice. 18

2.2 A single box 24

2.3 A pair of boxes, exchanging heat 24

2.4 A diagram showing the various fluxes incoming and outgoing from each box. 28

3.2 A plot of temperature vs. time of the two boxes when transport is not included in the model. Ice covered is indicated by a dashed line and open water is indicated by a solid line. 35

3.3 Temperature vs. time plot for parameter sweep for $k = 0, 1, 10, 50$. Open water is indicated by a solid line and ice-covered water is indicated by a dashed line. 37

3.4 The temperature difference between boxes for $k = 0, 1, 10, 50, 100, 500$. . . 38

3.5 Temperature vs. time plot for parameter sweep for $k_3 = 0, 1, 10, 50$. Open water is indicated by a solid line and ice-covered water is indicated by a dashed line. 40

3.6 The temperature difference between boxes for $k_3 = 0, 1, 10, 50, 100, 500$. . . 41

3.7 The dimensions of the boxes used to generate the results of the previous section. 42

3.8 Plot of temperature vs time for equal length boxes. 45

3.9 Plot of temperature vs. time for an open water box that has half the length of the ice covered box. 46

3.10 Plot of temperature vs. time for an ice covered box that has half the length of the open water box. 46

3.11 A plot of temperature vs. time for a day-night cycle where there is no emissivity switch. The vertical axis has a constant shift of $273K$. 49

3.12 Diagram of the emissivity switching values with the temperature change. . 51

3.13 A plot of temperature vs. time for a day-night cycle where an emissivity "switch" is in place. 52

4.1 Schematic of transport between four boxes as would be seen in a four-box model. 56

4.2 Relevant four-box model configurations for surface reflectivity. Other configurations, such as two side-by-side boxes with the same surface properties, would be a subset of the results shown in this thesis. 57

List of Tables

3.1 Parameter set for Section 3.2 44

Chapter 1

Introduction

1.1 Climate Change Impacts to Seasonal Cycling of Ice Cover

1.1.1 Ice Cover Trends and Implications

In 'Freezing of Lakes' by Matti Lepparanta [**?**], a climate zone referred to as the "cold climate zone" is defined. He proposes that the cold climate zone shall refer to the areas in the Northern and Southern Hemispheres that experience a period of time where their mean air temperature is less than $0°C$. Put simply, these are the areas of the Earth which experience a distinct cold season. While these areas are quite numerous in the Northern Hemisphere, there are very few in the Southern Hemisphere [**?**]. So, for the rest of this document we shall concern ourselves primarily with ice-covered lakes in the Northern

Hemisphere, and will refer to the "Northern Hemisphere" as the Northern portion of this "cold climate zone", which is roughly 45 degrees North of the equator.

Most small and medium-sized lakes in this Northern Hemisphere that we have defined traverse the same qualitative seasonal cycle every year. In late fall clear ice forms on the surface of the lake, which we will refer to as the "ice-on" date, then the amount of ice cover increases over the winter until the lake is completely or almost completely covered by ice [21]. Then in spring, some fraction of the ice cover melts and the ice breaks up, before finally melting completely on what we will call the "ice-off" date. When the lake is not completely ice free or fully covered by ice, the lake will be under partial ice cover (PIC). Historically, small and medium Northern Hemisphere lakes have spent most of the winter under a complete (or very nearly complete) and intact, cover of ice which limits the PIC season to two periods per year: the first, between the ice-on date and the date of full ice coverage, and then from the ice-breakup date to the ice-off date. Meanwhile, large lakes such as the Great Lakes may develop ice cover but often it will not be complete and in some years are virtually ice-free [15]. In the past 50 years numerous studies have shown that the seasonal cycle of lakes, in particular across Canada and Northern Europe, has seen significant changes due to climate change and so the PIC season could become longer.

Ice coverage duration has been shown to be decreasing due to climate change. Magnuson et al. [19] considered data from the 1846-1995 time period on lakes and rivers in Russia, Japan, and Finland and found that ice breakup dates were trending towards earlier appearances. In Canada, Duguay et al. [9] found that analysis of Canadian lake data from the 1990s showed ice-breakup dates trending earlier each year, however found no significant



Figure 1.1: A pond near University of Waterloo Health Services under varying stages of ice cover. Pictures were taken during January - March 2025.

change in ice freeze-up dates.

These findings alone indicate a shorter ice cover period for many Northern Hemisphere lakes. However, there are also indications that ice cover is becoming less extensive when it does occur. Sharma et al. [25] postulates that the number of lakes that currently experiences intermittent ice cover would more than double with a mean air temperature increase of 2 ° C, and many lakes at relatively southern latitudes are already experiencing intermittent ice cover. Meanwhile on the Great Lakes, Wang et al. [29] found that over the 1973-2012 period, ice cover on Lake Ontario has reduced 88 percent, Lake Superior 79 percent, and the total loss over all the Great Lakes (including Lake St. Clair) was 71 percent. These indications of less extensive ice cover, combined with the possibility of late freeze-up dates and early break-up dates, could mean that many Northern Hemisphere lakes spend more of their winters under PIC.

Lack of full ice cover and shorter ice cover seasons could have significant effects for those who depend on their local lake's seasonal cycle for economic activity. Some towns in Canada's far north rely on "ice roads", which are paths across lake ice that is thick enough for vehicles to pass over, to become road accessible [27, 11]. These winter roads help supply towns that would otherwise be cut off from road infrastructure have access to supplies in neighboring towns and airports. In Ontario, ice fishing around Lake Simcoe makes up a large proportion of total winter fishing and approximately 30 commercial ice fishing businesses operating from the lake depend on thick and complete ice cover [24]. Meanwhile, in more southern latitudes, shipping on the Great Lakes could be adversely affected by a longer ice-free season. Shorter ice seasons and lower ice cover fractions have

contributed to warmer lake temperatures, which increases evaporation from the lakes and lowers the water level [20]. A lower water level means that to remain within clearance limits ships must operate at reduced cargo payload, which would cause reduced efficiency and higher costs.

As well as the key role lakes have in facilitating commerce and business, they are also important to the health of those who live near them. The Great Lakes Commission states that 40 million Canadians and Americans rely on the Great Lakes to supply their drinking water [6]. Lake Erie is routinely plagued with blooms of cyanobacteria that contaminate drinking water, which Twiss et al. [28] posit could be limited by low sunlight conditions and low temperatures. Meanwhile, in Russia, Katz et al. [13] have shown a link to low albedo ice cover and the growth of harmful algal blooms in Lake Baikal. As well, Katz et al. [13] discuss the possibility of convective mixing in lakes helping to keep phytoplankton suspended in the lake's "photic zone", an area where algae are able to absorb enough sunlight to maintain photosynthesis.

Evidently, many academic efforts have been made to find trends in ice-on dates, ice-breakup dates, and ice coverage extent. Similarly, the impacts that ice loss could have on regional economics and lake health has no shortage of analysis. From these efforts it is clear that many lakes in the Northern Hemisphere are trending toward PIC in the winter rather than full ice cover, and this will have far reaching effects. However, there remains another natural phenomenon that increased prevalence of PIC could affect which has not seen the same volume of analysis: the weather. In their review paper "The Response and Role of Lake Ice Cover in Lake-Climate Interactions", Brown and Duguay [5] assert that

the incorporation of lake models "with or without lake ice components" into atmospheric models would improve regional weather predictions. Strengthening this point, Wright et al. [31] simulated three test scenarios with a weather forecasting model to ascertain the effect of ice cover and warmer lake surface temperatures on "lake-effect snowfall". It was found that while complete ice cover eliminates the lake's influence on snowfall, warmer lake temperatures increased the area affected by the lake-effect. Notably, the local distribution of the lake-effect snowfall was significantly impacted by the lake surface temperature.

The wintertime life cycle of Northern Hemisphere lakes has been significantly impacted by climate change. Changes to ice-on, ice-off, and ice-breakup dates are present across Canadian and Northern European latitudes, indicating that the prevalence of PIC during the winter will increase. With lakes not completely covered by ice for the winter, the possibility for heightened lake-effect snowfall will also likely increase. In most studies of lake-effect, lakes are typically treated as either fully covered by ice or ice free [5]. While it may seem a reasonable approximation to assume that a lake covered by PIC is effectively the same as ice-free, PIC can have unexpected consequences on the flow behaviour of the lake which can in turn impact its surface temperature. In particular, effects of PIC on radiatively driven convection are virtually unstudied due to the high level of complexity posed and the inherent difficulty of measurement in this setting. However, in today's climate landscape it is crucial to consider radiatively driven convection under partial ice cover to gain a more realistic picture of the wintertime limnology of our Northern Hemisphere lakes.

1.1.2 Radiatively Driven Exchange

We have now discussed that ice cover extent and the flow dynamics it produces are important to not only the regional economy, but also to a lake's overall water quality. As well, it is clear that the weather in regions around lakes is strongly impacted by the lake surface temperature. Despite the clear reduction in ice cover extent, many studies still assume complete ice cover when considering a lake's wintertime limnology, which could instigate an incomplete understanding of the fluid motion and subsequent biological processes. A main feature of PIC that is rarely considered is its effect on radiatively driven convection (RDC).

Lake ice is typically seasonal, but as long as it can persist into the winter it can usually become snow covered. Snow has a high albedo, meaning it reflects the majority of its incident solar radiation [**?**]. During times of full ice coverage, this high reflectivity and protection from wind allows the water beneath snow covered ice to stay very cold; within the temperature range between 0 °C and water's temperature of maximum density, $T_{md} = 4°C$ [4]. We will refer to this temperature range as the "cold water regime". However, water has a very low albedo [**?**] and so open water easily absorbs solar radiation, which in turn rapidly increases its temperature. Water has a nonlinear equation of state, meaning it is most dense at the previously mentioned value of T_{md} and decreases in density for temperatures greater and less than this value. A plot of water's equation of state is shown in Figure 1.2 and the temperature range highlighted in blue is the cold water regime where increasing temperature increases density.

Because in the cold water regime heating water also increases its density, radiatively

driven convection can have more interesting effects on the stratification of a lake than if the lake was warmer than the temperature of maximum density. Typically radiatively driven convection in the cold water regime occurs when the sun heats the surface, whose temperature is less than T_{md}, and increases its temperature and therefore density so that this surface fluid sinks and colder, less dense fluid rises [4]. Radiatively driven convection is a primarily vertical process. However, in the case of partial ice cover, horizontal convection is possible between the warm, dense zones of open water and the adjacent cold, ice-covered regions [2]. We will refer to this PIC-induced flow as "radiatively driven exchange" (RDE).

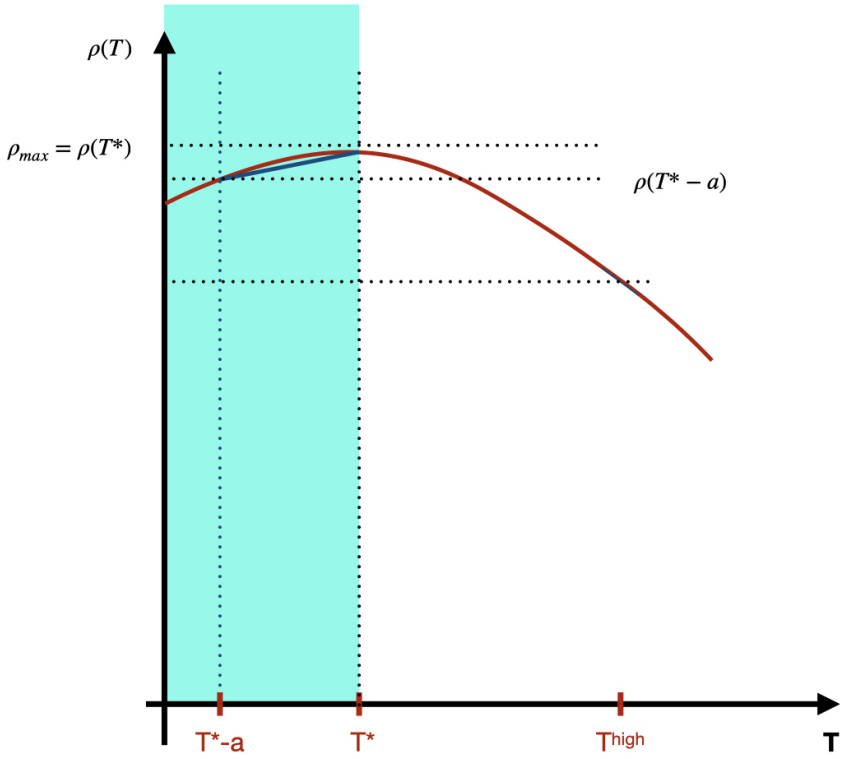


Figure 1.2: Plot of water's equation of state. Temperature of maximum density is marked and the cold water regime is highlighted in blue.

It is clear from the need for a new terminology that RDE is an extremely unstudied topic. Allum & Stastna [2] studied buoyancy-driven flows under ice cover with nonuniform optical properties and found that there is indeed gravity current-like flow between areas of strong and weak solar radiation absorption. Three dimensional simulations were run with a "shadow" of low insolation absorptivity in two different shapes: the first, a quarter circle situated in the corner of the tank, and the second, a rectangular strip that fully covered one side of the simulation tank. An averaged schematic of the results of these simulations are depicted below, with mixing between the shadowed and unshadowed regions evident. It must be assumed then that the described mixing must be occurring in lakes with partial ice cover, as PIC induces drastic spatial disparities in absorptivity of insolation.

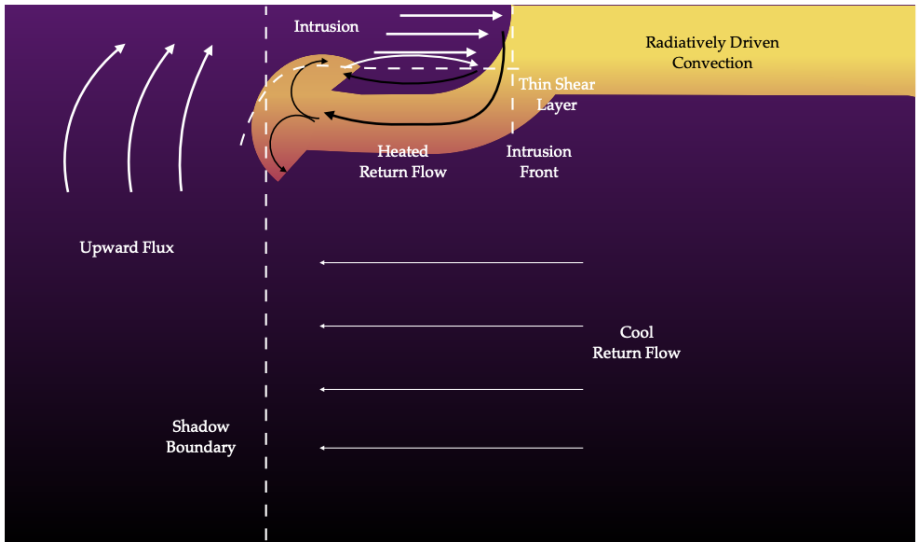


Figure 1.3: Schematic of the results found in Allum et al. [2]. The schematic shows a side view of the mixing that takes place between areas of low and high insolation absorption. Figure is taken from [2].

The mixing shown between zones of high and low insolation absorption will likely affect the temperature of a lake under PIC. So to model these lakes, it is crucial to include this inter-zone exchange to get the most accurate results. However, repurposing an existing model to include horizontal transport is complicated as lake temperature models usually focus on vertical stratification. Therefore, it becomes very difficult, or at least computationally inefficient, to also include horizontal mixing. We will discuss in the next section some lake temperature models and their intended use, as well as their potential to resolving horizontal transport.

1.2 Existing Models

There exist some prominent lake temperature models that are well-used in numerical weather prediction and other applications. Discussed here are models FLake and CLIMo, developed in Germany and Canada respectively, which have both made significant progress in accurately but efficiently modelling freshwater lake temperatures.

1.2.1 FLake

FLake is a freshwater lake parameterization scheme that is used widely in numerical weather prediction across Europe, described in [22]. It has also been applied to other forms of climate modelling. The goal of FLake is to calculate the evolving surface temperature profile of freshwater lakes for very short or very long time scales [22]. The concept of self-similarity in the temperature profile is used to separate the depth of the lake into an

upper mixed layer and a lower bottom layer, and temperature profiles are calculated for both [22]. This concept is used as an attempt to dispel the errors that come from ignoring lake stratification and assigning a single temperature to the entire water column, while still retaining computational efficiency. The lake is separated into "zones" vertically, but is considered as a single expanse horizontally. FLake accounts for many factors that could affect a lake's temperature, including the interaction of the water with bottom sediments and the effects of ice and snow. However, there does not appear to be much consideration for partial ice cover or ability to resolve the horizontal transport it introduces. FLake assumes either complete ice cover or open water.

1.2.2 CLIMo

CLIMo, or Canadian Lake Ice Model, is a one-dimensional thermodynamic model that describes a lake's temperature as it depends on time and depth [8]. CLIMo uses a finite difference scheme to solve the partial differential equation

$$\rho C_p \frac{\partial T}{\partial t} = \frac{\partial}{\partial z} k \frac{\partial T}{\partial z} + F_{sw} I_0 (1 - \alpha) K e^{-Kz} \tag{1.1}$$

where ρ is the density of water, C_p is its heat capacity, F_{sw} is the shortwave radiation flux from the Sun, α is the surface albedo, and I_0 is the fraction of the shortwave radiation that gets through the ice [8]. CLIMo is primarily concerned with the vertical structure of a lake, and is very thorough in its consideration of the various properties that affect a lake's stratification. As well, care is taken to ensure that ice growth can be simulated in the model. The purpose of CLIMo is primarily to predict ice-on and ice-off dates and to

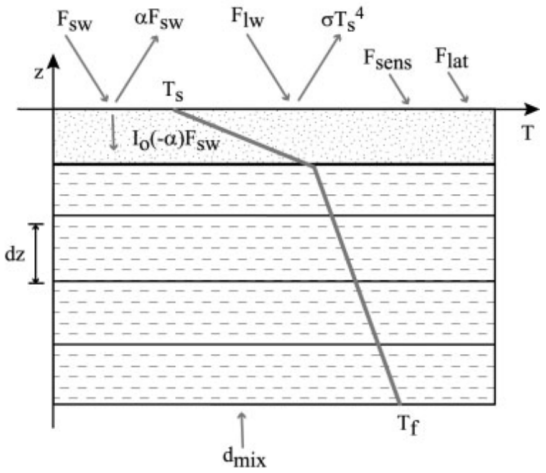


Figure 1.4: From Duguay et al.[8], a schematic of the various surface fluxes considered in CLIMo.

compare this to in-situ measurements [8]. It is extremely successful and well-tested in this application. For the purposes of allowing mixing between areas of ice cover and open water however, its crucial dependence on its one-dimensional structure (z only) makes it a poor candidate for studies of mixing due to PIC.

1.3 Box Models

Box models are particularly useful for considering fluxes into and out of a cubic volume. They are widely used in physical modelling as a way to consider the broad overviews of complex systems. Box models are used frequently in air quality modelling [12] and also have fluid mechanics applications. One example of a famous box model is the Stommel model, which was developed to study the changes in the thermo-haline current (THC) [14],[26].

The THC is an ocean circulation current that is driven by density differences in adjacent zones of sea water [14]. Stommel's model is an idealized version of the physical reality, where two well-mixed boxes with different temperatures and salinities are exchanging parcels of water between them due to their density difference [26]. The purpose of Stommel's model is to model evolution of each box's temperature and salinity in time. Our model follows in the footsteps of Stommel's work in a freshwater setting by including transport due to density differences between boxes to analyze the temperature in time.

1.4 Model Description and Goal

A lake's surface temperature is an important variable. It can help predict weather and algal contamination, among other things. In the models described so far, it is clear that most lake temperature models have poor ability to resolve the complexities of partial ice cover and where they do, it is near impossible to incorporate the horizontal transport and mixing that Allum et al. [2] have shown. Here we follow in the steps of a model that includes mixing between zones, the Stommel box model, to create a simple model that is capable of capturing the transport between zones of open water and ice cover. The goal of the model presented in this thesis is to provide an "as simple as possible" box model that simulates the temperature of a freshwater lake under partial ice cover by incorporating surface energy fluxes and horizontal heat transport between zones with contrasting surface properties. The temperature of the water column is assumed to be constant for each box and focus is placed instead on the temperature differences between zones of open water and ice cover.

1.5 Thesis Outline

The second chapter serves as an introduction to surface energy fluxes such as radiation from the Sun and outgoing longwave radiation that is emitted by the boxes, as well as the absorption and emission capabilities of water and snow-covered ice. The third chapter covers results of the model, which are split into constant insolation results that focus on temperature steady states, and day-night cycle results which focus on the model's behaviour when insolation is cycling. In the results section efforts are made to prioritize the simplicity of the model while maintaining realistic results and behaviours. The fourth chapter discusses conclusions and suggests avenues for future work.

Chapter 2

Technical Background and Model Derivation

2.1 Radiation

Radiation, whether it is emitted or absorbed, is the foundation of energy balance models. In the case of our model, the incoming radiation from the Sun is counterbalanced by the radiation that each box emits. Every object interacts with radiation differently. Some objects are excellent at absorbing and emitting radiation, whereas others do not absorb high levels of radiation and instead reflect it. At the core of the model presented in this thesis lie the differing radiative properties of water and ice. That their individual abilities to absorb and emit radiation are dissimilar causes the temperature difference between them. The purpose of this section is to provide a general overview of incoming and outgoing

radiation, as well as the absorption, emission, and reflection properties of water and ice.

2.1.1 Incoming Radiation

The "incoming" radiation considered here is radiation from the Sun that is incident upon the surface of each of our boxes. It is the main source of heat in our model. The Sun radiates at all wavelengths of the electromagnetic spectrum, but only a few make it through the Earth's atmosphere, so most climate energy balance models only consider radiation in the UV and infrared spectrum [23]. The power of the total radiation of the Sun, Q, given off in all directions is in the range of 1370 W/m^2 [4]. An approximation of the total power of the radiation incident on the Earth in the Northern Hemisphere is 1370/4 W/m^2.

When radiation is incident upon a surface, it can be reflected, absorbed, or transmitted [23]. We do not consider radiation transmission here, as it is not an important factor in the overall energy balance of either box. Instead, we focus on the reflectivity and absorptivity which are major components in what drives the temperature difference between the boxes. When solar radiation contacts the surface of the lake, it causes the water molecules to move faster and therefore increases the temperature of the water column [1]. The amount the temperature increases depends on how much radiation is absorbed [1].

Absorptivity is a unitless parameter that is defined as the ratio of incident radiation that is absorbed into a surface to the total radiation incident upon a surface [23]. So it is the fraction of radiation absorbed into the surface. Meanwhile, since transmissivity is not considered here, radiation that is not absorbed can only be reflected in all directions away from the surface. It follows intuitively that the reflectivity is then not only the ratio of

incident radiation that is reflected away from a surface to the total radiation incident, but it is also equal to $1-\alpha$ where α is the absorptivity [23]. Similarly, the fraction of radiation absorbed can be written as $1-a$, where a is the albedo. The reflectivity of a surface is often referred to as "albedo", and that is what we shall call it in some sections of this text.

Water and ice have very different absorptive and reflective profiles, which are depicted in Figure 2.1. Also, because absorptivity and emissivity are linked by Kirchoff's law of thermal radiation which says that the absorptivity is equal to the emissivity [23], water and ice have very different emissivities. Water is very nearly a black body [23], as it absorbs the vast majority of radiation that is incident upon it, and it emits nearly the maximum possible radiation. Meanwhile, ice can be highly reflective depending on its composition and level of snow cover [17]. We assume in this text that our ice is very reflective, to maximize the difference in surface properties between the open water box and the ice-covered box.

Because a significant portion of all incident radiation on the ice is reflected, little radiation is absorbed by it. Its low absorptivity translates to low emissivity and so ice also emits much less radiation than water. So, open water will readily heat up when the sun is on it but it will cool just as easily at night. In contrast, ice-covered water will have a "lid" on it so that it is not so easily heated during the day time, but it is also not so easily cooled at night. These behaviours drive the temperature difference between the two boxes in the model.

We have now established that the total insolation on a surface is $Q/4$ and we have discussed that the fraction of this amount that is absorbed into the surface depends on the

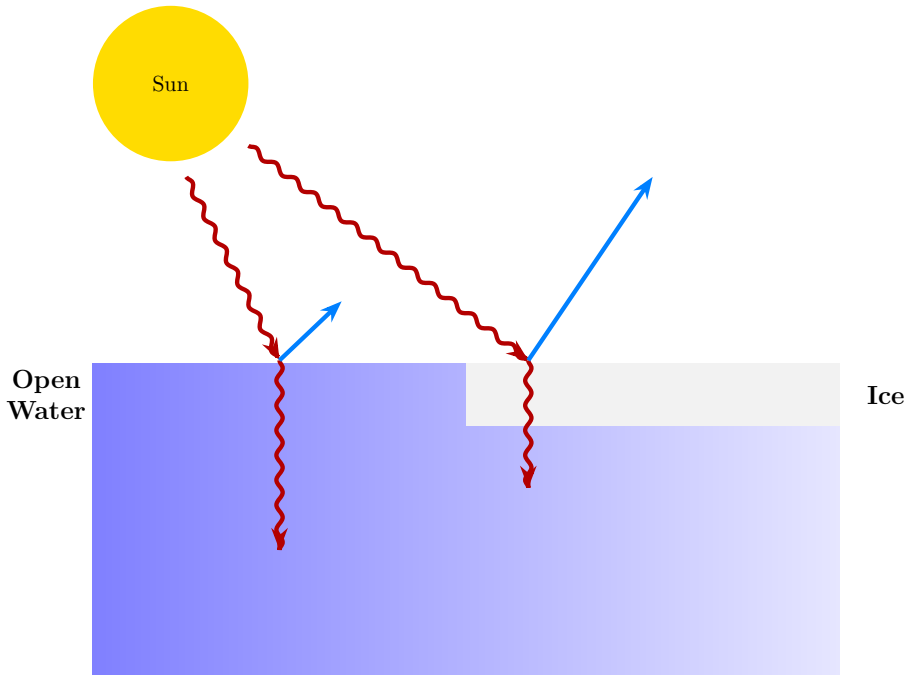


Figure 2.1: A diagram depicting the absorptive behaviours of water and ice.

albedo. So, we can approximate the amount of radiation absorbed by each surface by

$$q_{in} = \frac{Q}{4}(1 - a_i) \tag{2.1}$$

where Q is the total power of the Sun and a_i is the albedo of either open water or ice.

2.1.2 Outgoing Radiation

All objects emit radiation. While each box in our model gains heat by absorbing incident solar radiation, it loses heat by emitting radiation. We will sometimes refer to radiation emitted by an object as "outgoing" radiation because it is leaving the object emitting it. Emitting radiation is particularly impactful to the temperature of each box at night, when incoming radiation from the Sun is not present to counterbalance the outgoing radiation emitted from each of the boxes.

The amount of radiation that an object emits depends on the object's temperature and emissivity as defined by the Stefan-Boltzmann law ([23]). This law states that the amount of radiation emitted by a black body is given by

$$B(T) = \sigma T^4 \tag{2.2}$$

where σ is the Stefan-Boltzmann constant and T is the temperature (°K). A black body is an idealized object, used often in physics, that is both a perfect absorber and emitter of radiation. Although a black body is the object considered for Equation 2.2, the black body's property of being a perfect emitter means that Equation 2.2 represents the maximum

possible radiation emitted from any object. However, the black body is an idealized object and such prodigious absorption and emission of radiation does not exist. Instead, realistic objects emit some fraction of Equation 2.2. This fraction is the emissivity, which is defined as the ratio of radiation emitted by a body to the total possible radiation emitted. Then, the amount of radiation emitted for a realistic object can be written as the amount of radiation emitted from a black body multiplied by the emissivity, given by ϵ, as in Equation 2.3.

$$R(T) = \epsilon\sigma T^4 \tag{2.3}$$

2.2 Transport

The transport of heat between boxes is the most unique component of the model. Most models of partial ice cover do not consider the exchange of heat between ice cover zones and open water. However, where there is a temperature difference, there will be exchanges between these zones. The exact mechanism with which heat is transported between zones is likely a combination of convection and conduction, but because thermal conduction in water is much slower than heat transfer via convection and we have confirmed flow between zones, we focus on the aspect of convective heat transfer here. Convection is driven by the buoyancy forces that arise from density differences in fluids. If a denser fluid is atop a fluid that is less dense than it, gravity will set the fluid in motion. This type of convection is often called "free" convection.

The equation of state of water's density is a formula that describes how the density

of water, ρ, depends on the temperature, T and the pressure, p. In the absence of large pressure changes, we can just examine the relationship between temperature and density. Generally, fluids lose density as they gain temperature, but this is not exactly true for water. Water's equation of state is approximately a negative quadratic, with its peak occurring at $T_{md} \approx 4°C$ or 277 K. So water is at its most dense at approximately $4°C$ and is less dense at temperatures greater and less than this value, as seen in the plot in 1.2 We then expect that partial ice cover can give rise to sideways mixing between zones of ice cover and open water, because the temperature difference between them will translate into a density difference. Evidence of this horizontal transport is confirmed in [2].

Convective heat transfer follows Newton's law of cooling, which is

$$q_{transport} = kA\Delta T \tag{2.4}$$

where ΔT is the difference in temperature between the body studied and the object with which is it exchanging heat (K), A is the area over which they are in contact (m^2), and k is the convective heat transfer coefficient $(W/(m^2 \cdot K))$. To determine k, the properties of the fluid must be considered, as well as the direction of flow. An exact value for k is not calculated in this thesis. Instead, it is treated as a tunable parameter which is modified to achieve reasonable results.

In addition to Equation 2.4 and its linear dependence on ΔT, we also will add a term that describes convective heat transport with a nonlinear dependence on ΔT,

$$q_{transport} = k_3 A(\Delta T)^3 \tag{2.5}$$

where ΔT and A are as in Equation 2.4, but k_3 is now the nonlinear convective heat transfer coefficient which has units of $(W/(m^2 \cdot K^3))$. The exact value of k_3 is not calculated in this thesis and it is treated in the same fashion as k. The role of Equation 2.5 in the model is to add realism to the results by introducing stronger mixing. The purpose and necessity of nonlinear transport is discussed further in section 3.1.

2.3 Building the Model

In this final section of our Methods chapter, we will derive our simple model for temperature under partial ice cover with heat transport between zones. We will begin with the derivation of the equations from calculus rules and then simplify the model by nondimensionalizing it while assuming the temperatures are in steady state.

2.3.1 Derivation

Total Heat of a Single Box

Consider a cube with dimensions as shown in Figure 2.2: height H (m), width W (m), and length L (m). The total heat, $q(t)$, in a box of this size filled with some medium is given by

$$q(t) = \int_0^H \int_0^W \int_0^L \rho c_p \, T(x, y, z, t) \, dx \, dy \, dz \tag{2.6}$$

where ρ is the density of the medium (kg/m^2), c_p is the heat capacity of the medium ($J/(kgK)$), and T is the temperature distribution in the box which is a function of x, y, z, t. We can also write Equation 2.6 in terms of the average temperature in the box, so that we have

$$q(t) = \rho c_p V \langle T(t) \rangle \tag{2.7}$$

where $\langle T(t) \rangle$ represents the average temperature over the volume of the box at time t and V is the volume of the box, which in the case of the cube in Figure 2.2 is equal to WLH. We will refer to $\langle T(t) \rangle$ simply as T for the rest of this text for simplicity. Meanwhile, we know that the rate of change of the total heat in the box is equal to the total internal change plus the heat coming into the box minus the heat released from it, as follows:

$$\frac{\mathrm{d}q}{\mathrm{d}t} = q_{internal} + q_{in} - q_{out} \tag{2.8}$$

The total internal change is given by $q_{internal}$ (W), which describes whether there is a heat source or heat sink within the box, the total incoming heat is given by q_{in} and the total outgoing heat is given by q_{out}. Let us assume that our box is a box of lake water with no heat source or sink, and the external fluxes it experiences are the same as an average Canadian lake. Then, we have established in section 2.1.1 that the magnitude of the heat entering the box would be the incoming radiation from the Sun, which is equal to

$$\frac{Q}{4}(1 - a) \tag{2.9}$$

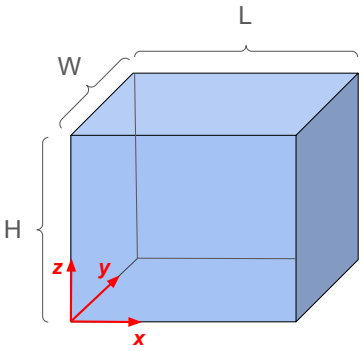


Figure 2.2: A single box

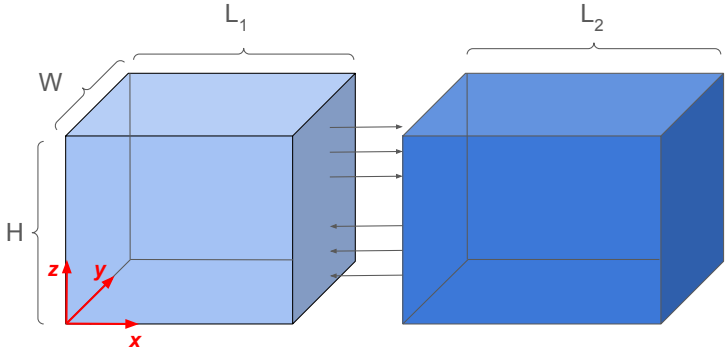


Figure 2.3: A pair of boxes, exchanging heat

where Q is the total energy produced by the Sun (W/m^2) and a is the albedo of the surface upon which the insolation is incident.

We also know from previous sections that all objects will radiate in accordance with the Stefan-Boltzmann Law of radiation [23], so the heat exiting our lake-box will be equal to

$$\epsilon\sigma T^4 \tag{2.10}$$

with emissivity as described in Section 2.1. Recall that T refers to $\langle T(t)\rangle$.

Since both the incoming and outgoing heat fluxes in Equations 2.9 and 2.10 pass through the top of our cube and have units of (W/m^2), the total rate of incoming heat must be given by

$$q_{in} = \frac{Q}{4}(1-a)(WL) \tag{2.11}$$

and the total rate of change of outgoing heat must be

$$q_{out} = \epsilon\sigma T^4(WL) \tag{2.12}$$

Then, we can write the rate of total heat of a single box as

$$\frac{\mathrm{d}q(t)}{\mathrm{d}t} = \left(\frac{Q}{4}(1-a) - \epsilon\sigma T^4\right) WL \tag{2.13}$$

Then, substituting Equation 2.7 into the left-hand side of Figure 2.13, we have

$$\rho c_p V \frac{\mathrm{d}T}{\mathrm{d}t} = \left(\frac{Q}{4}(1-a) - \epsilon\sigma T^4\right) WL \tag{2.14}$$

and simplification gives

$$\frac{\mathrm{d}T}{\mathrm{d}t} = \frac{\frac{Q}{4}(1-a) - \epsilon\sigma T^4}{\rho c_p H} \tag{2.15}$$

A Pair of Boxes

Now let us expand our situation to include a second box alongside the first. The second box has a width and height equivalent to the first box, but its length L_2 is not constrained to be equal to the length of the first box, L_1. As depicted in Figure 2.3, the two boxes will exchange heat through their shared side, of area WH. As discussed in section 2.2, heat transport is described by the functions $k\Delta T$ and $k_3\Delta T$, where ΔT is the temperature difference between the boxes. We now must consider a pair of coupled ordinary differential

equations, one for the rate of change of temperature for the first box and one for the rate of change of temperature for the second box. These are linked due to the heat exchange between the two boxes. For example, if the second box is warmer than the first, it will "give" heat to the first box and this will affect the rate of change of the first box's temperature. The signs of ΔT and ΔT^3 determine whether the heat is heat taken or given to a particular box.

We can describe the rate of change of heat over time between the boxes as we did in the previous sections, where the transport is multiplied by the area of the shared side:

$$\frac{\mathrm{d}q_{transport}}{\mathrm{d}t} = (k\Delta T + k_3\Delta T^3)(WH) \tag{2.16}$$

So, adding transport to Equation 2.15 and considering two boxes gives us

$$\frac{\mathrm{d}T_1}{\mathrm{d}t} = \frac{1}{\rho c_p}\left(\frac{(\frac{Q}{4}(1-a_1) - \epsilon_1\sigma T_1^4)}{H} + \frac{(-k(T_1-T_2) - k_3(T_1-T_2)^3)}{L_1}\right) \tag{2.17}$$

with the same equation holding for the second box,

$$\frac{\mathrm{d}T_2}{\mathrm{d}t} = \frac{1}{\rho c_p}\left(\frac{(\frac{Q}{4}(1-a_2) - \epsilon_2\sigma T_2^4)}{H} + \frac{(-k(T_2-T_1) - k_3(T_2-T_1)^3)}{L_2}\right) \tag{2.18}$$

If we are to consider these equations when the temperatures are in steady state, then we will have

$$\frac{(\frac{Q}{4}(1-a_1) - \epsilon_1\sigma T_1^4)}{H} + \frac{(-k(T_1-T_2) - k_3(T_1-T_2)^3)}{L_1} = 0 \tag{2.19}$$

and

$$\frac{\left(\frac{Q}{4}(1-a_2)-\epsilon_2\sigma T_2^4\right)}{H}+\frac{(-k(T_2-T_1)-k_3(T_2-T_1)^3)}{L_2}=0 \tag{2.20}$$

Parameter Considerations

In Equations 2.17 and 2.18 we note that the albedo, a, and emissivity, ϵ, are box-specific, but density ρ and heat capacity c_p are not. This is because we are assuming one of the boxes is covered by ice. This affects the albedo and emissivity values between boxes because the ice acts as a "radiation lid" on the second box. Its high albedo prevents solar radiation from heating the water beneath it, and its low emissivity decreases the rate at which the water below cools. However, below the surface, the medium that both boxes are filled with is water and the ice that covers one of the boxes is assumed to not contribute significantly to its volume. So, the density and heat capacity used in Equations 2.6 and 2.7 do not change between boxes.

A complete diagram of the situation with each term is given in Figure 2.4.

2.3.2 Simplification

In this section, we simplify our model by scaling its parameters while it is in steady state. This allows us to write the parameters in groups for easier analysis.

We shall work just with Equation 2.19 for a moment. Factoring k from the transport terms gives

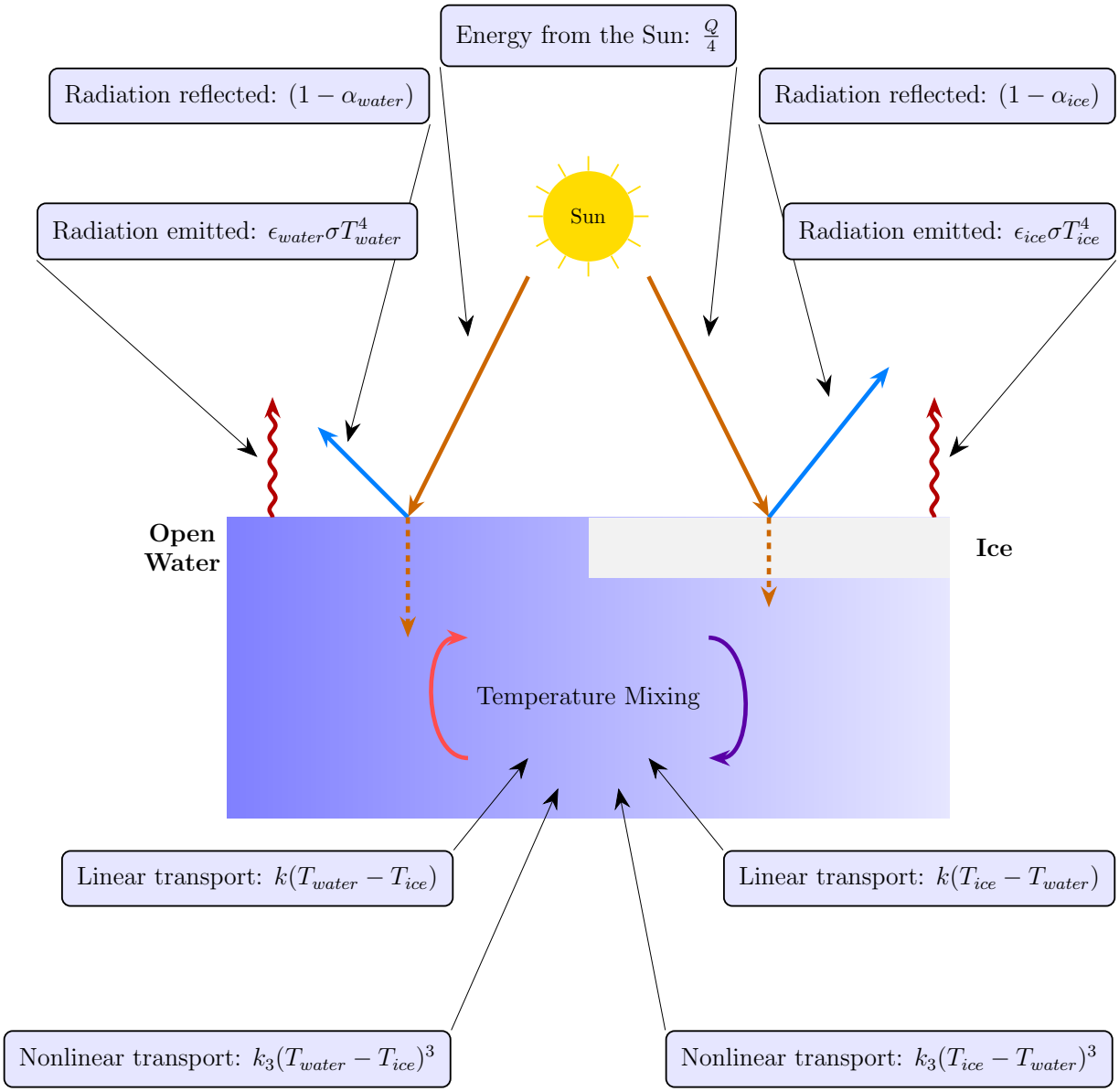


Figure 2.4: A diagram showing the various fluxes incoming and outgoing from each box.

$$\frac{(\frac{Q}{4}(1-a_1)-\epsilon_1\sigma T_1^4)}{H}-\frac{k}{L_1}((T_1-T_2)+\frac{k_3}{k}(T_1-T_2)^3)=0 \tag{2.21}$$

Then, let us divide the equation by the energy from the Sun, $\frac{Q}{4}(1-a_1)$, so we get

$$\frac{1}{H}(1-\frac{\epsilon_1\sigma}{\frac{Q}{4}(1-a_1)}T_1^4)-\frac{k}{L_1\frac{Q}{4}(1-a_1)}((T_1-T_2)+\frac{k_3}{k}(T_1-T_2)^3)=0 \tag{2.22}$$

Let $A_1=\frac{\epsilon_1\sigma}{\frac{Q}{4}(1-a_1)}$, $B_1=\frac{k}{\frac{Q}{4}(1-a_1)}$, and $\beta=k_3/k$. Then it is easier to write Equation 2.22 as

$$(1-A_1T_1^4)-\frac{B_1H}{L_1}((T_1-T_2)+\beta(T_1-T_2))=0 \tag{2.23}$$

Equation 2.20 can also be written in this way. If we divide by the energy of the Sun from the first box, $\frac{Q}{4}(1-a_1)$, we get:

$$\frac{1}{H}(\frac{(1-a_2)}{(1-a_1)}-\frac{\epsilon_2\sigma T_2^4}{\frac{Q}{4}(1-a_1)})-\frac{k}{L_2\frac{Q}{4}(1-a_1)}((T_2-T_1)+\beta(T_2-T_1)^3)=0 \tag{2.24}$$

Then, we can multiply both sides of the equation by $\frac{1-a_1}{1-a_2}$, so that we get:

$$\frac{1}{H}(1-\frac{\epsilon_2\sigma T_2^4}{\frac{Q}{4}(1-a_2)})-\frac{k}{L_2\frac{Q}{4}(1-a_2)}((T_2-T_1)+\beta(T_2-T_1)^3)=0 \tag{2.25}$$

Now, following a similar convention to the variable naming in Equation 2.23, let

$$A_2=\frac{\epsilon_2\sigma}{\frac{Q}{4}(1-a_2)} \tag{2.26}$$

and

$$B_2 = \frac{kH}{\frac{Q}{4}(1 - a_2)} \tag{2.27}$$

and β is as before. Then Equation 2.25, which was scaled by the same factor as Equation 2.23, can be written as

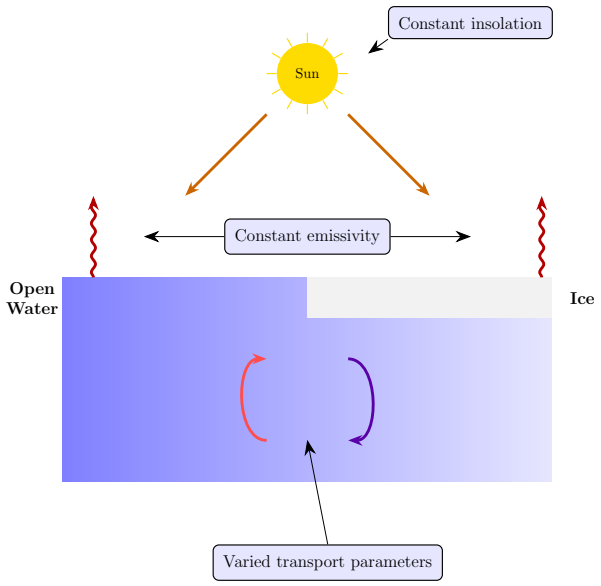
$$(1 - A_2 T_2^4) - \frac{B_2 H}{L_2}((T_2 - T_1) + \beta(T_2 - T_1)^3) = 0 \tag{2.28}$$

Equations 2.23 and 2.28 allow us to consider the model in a simpler form. By scaling the equation and grouping parameters, it can be easier to analyze which ones are important to the model. However, this thesis will focus on dimensional models and simulations.

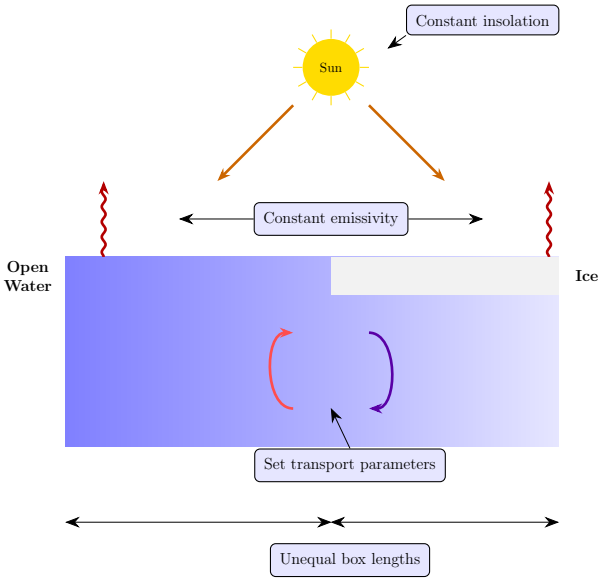
Chapter 3

Results and Discussion

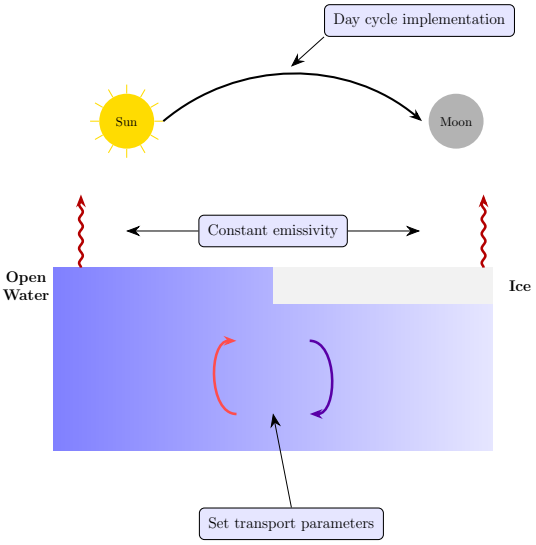
In this chapter, we review results for several versions of the model starting with the most basic and ending with the most complete. Discussions of results are included in each section. All of the models presented here are in dimensional form. The following figures describe how complexity is added into the model throughout the results section. Figures 3.1a and 3.1b pertain to the first section, where insolation is constant but parameters k and k_3, then the box length, are varied. Figure 3.1c pertains to Section 3.3.1, where we add a day cycle instead of holding insolation constant. Finally, Figure 3.1d shows the change from a day cycle with constant emissivity to a day cycle with an emissivity switch analyzed in Section 3.3.2.



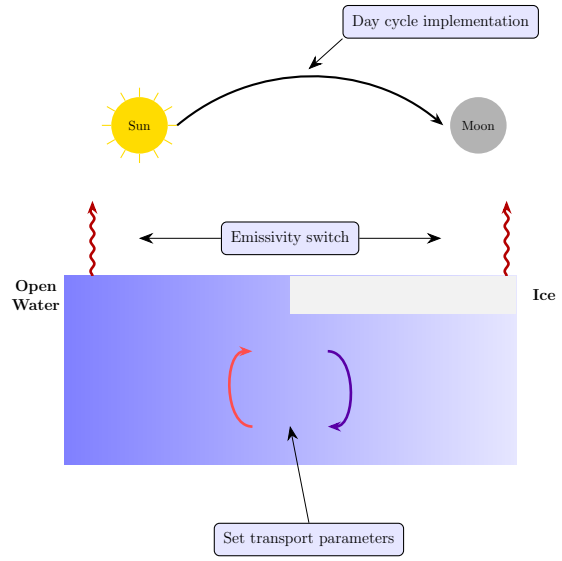
(a) Schematic of the situation modelled in Section 3.1.



(b) Schematic of the situation modelled in Section 3.2.



(c) Schematic of the situation modelled in Section 3.3.1.



(d) Schematic of the situation modelled in Section 3.3.2.

3.1 Constant Insolation Framework

The first simulations that we will analyze are those that have constant sunlight. In this scenario, the sun is always "on" and is supplying the model with the same level of heat at all times. While this situation is not reflective of a realistic lake at most Canadian latitudes and seasons, which would be subjected to cycles of day and night, it is a convenient framework in which to test the relative values of k, the linear transport parameter, and k_3, the nonlinear transport parameter. Most of the analysis in this section focuses on achieving reasonable temperatures when the model is in steady state. To allow for clear plots and shorter code runtimes, the value of the volumetric heat capacity ρc_p is set to 10^4 $(J/(kg \cdot K))$ which is lower than its actual value for water, 4.184×10^6 $(J/(kg \cdot K))$. For our steady-state analysis in a constant sunlight framework, the cancellation of the density and heat capacity terms in Equations 2.19 and 2.20, as well as the results of [18] means that the value of the heat capacity will not affect the temperatures at steady state. Instead, the effect of the heat capacity lies in the time required to reach steady state. For a ρc_p value of 4.184×10^6 $J/(kg \cdot K)$, the time to reach steady state is significantly longer than that of a lower ρc_p value. So, for the steady-state analysis in this section we will use the lower ρc_p value of 10^4 $J/(kg \cdot K)$. To avoid confusion, we explicitly note that the time to reach steady state as determined by ρc_p is of no relevance in this section since we are only using the numerical method here as a way to find the steady states that do not depend on ρc_p.

3.1.1 Model Without Transport

First we will examine the most basic version of the model, which is a pure energy balance model that does not include transport between boxes. The governing equations for this model are

$$\rho c_p V \frac{\mathrm{d}T_{ice}}{\mathrm{d}t} = (\frac{Q}{4}(1 - a_{ice}) - \epsilon_{ice}\sigma T_{ice}^4)LW \tag{3.1}$$

$$\rho c_p V \frac{\mathrm{d}T_{water}}{\mathrm{d}t} = (\frac{Q}{4}(1 - a_{water}) - \epsilon_{water}\sigma T_{water}^4)LW \tag{3.2}$$

The results of this model are shown in Figure 3.2. The model was run for 30 days with only the energy balance terms included. Both boxes are initially set to the same temperature: $275K$. The steady-state value for open water is greater than $285K$, while ice-covered water settles near a value of $265K$, which puts the temperature difference between the boxes at greater than twenty degrees. Although these steady-state values are certainly unphysical, they are not unexpected. In the absence of any mixing under the surface, each box will simply increase or decrease in temperature until the outgoing radiation term, $\epsilon\sigma T^4$, is equal to the incoming radiation, $\frac{Q}{4}(1 - a)$. This indirectly causes the albedo and emissivity of the surface to be in control of the steady-state temperatures. So, we see a large difference in the temperatures of the boxes and unrealistic steady-state temperatures when the model does not include mixing.

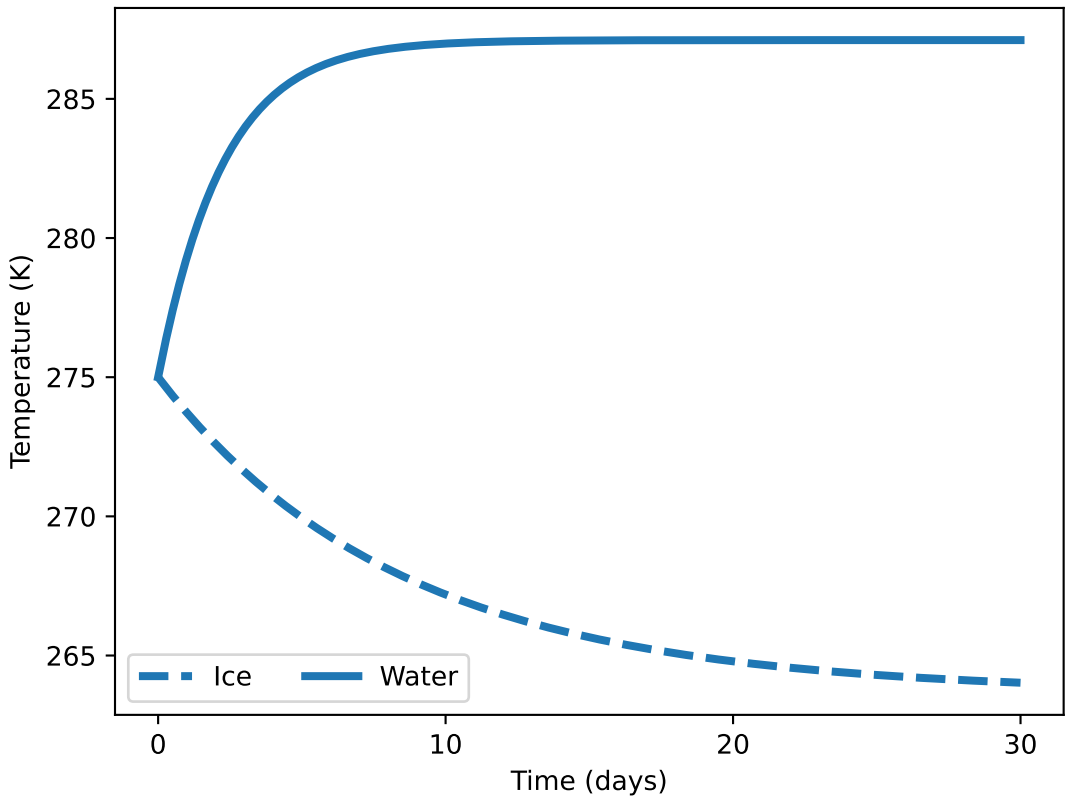


Figure 3.2: A plot of temperature vs. time of the two boxes when transport is not included in the model. Ice covered is indicated by a dashed line and open water is indicated by a solid line.

3.1.2 Linear Transport

The next model considered in the constant sunlight framework is one that includes only linear transport between boxes. The governing equations of this model are the following:

$$\rho c_p V \frac{\mathrm{d}T_{ice}}{\mathrm{d}t} = (\frac{Q}{4}(1 - a_{ice}) - \epsilon_{ice}\sigma T_{ice}^4)LW - k(T_{ice} - T_{water})WH \tag{3.3}$$

$$\rho c_p V \frac{\mathrm{d}T_{water}}{\mathrm{d}t} = (\frac{Q}{4}(1 - a_{water}) - \epsilon_{water}\sigma T_{water}^4)LW - k(T_{water} - T_{ice})WH \tag{3.4}$$

k is the convective heat transfer coefficient, with units of $W/(m^2 \cdot K)$. The exact value of k is dependent on several different factors, such as the type of flow and the properties of the fluids mixing. As k is not calculated exactly in this thesis, a sweep of values is performed to find which values of k can give realistic steady-state temperatures for both the open-water and ice-covered boxes, while also driving a reasonable level of mixing between them. Temperature difference will be used as an indicator of how strong the mixing between boxes is.

In Figure 3.3, we have plotted the temperature sets for four different values of k: $0, 1, 10$, and 50. The model was run for 14 days and both boxes started at initial temperatures of $275K$. The figure shows that while reasonable steady-state temperatures can be achieved for $k = 50$, the other values do not give reasonable temperatures and have the temperature of the ice-covered box below freezing. In addition, the results for $k = 0$ and $k = 1$ are nearly identical. For $k = 10$ the results are distinct from the smaller transport parameter values, but the steady-state results are still physically unfeasible.

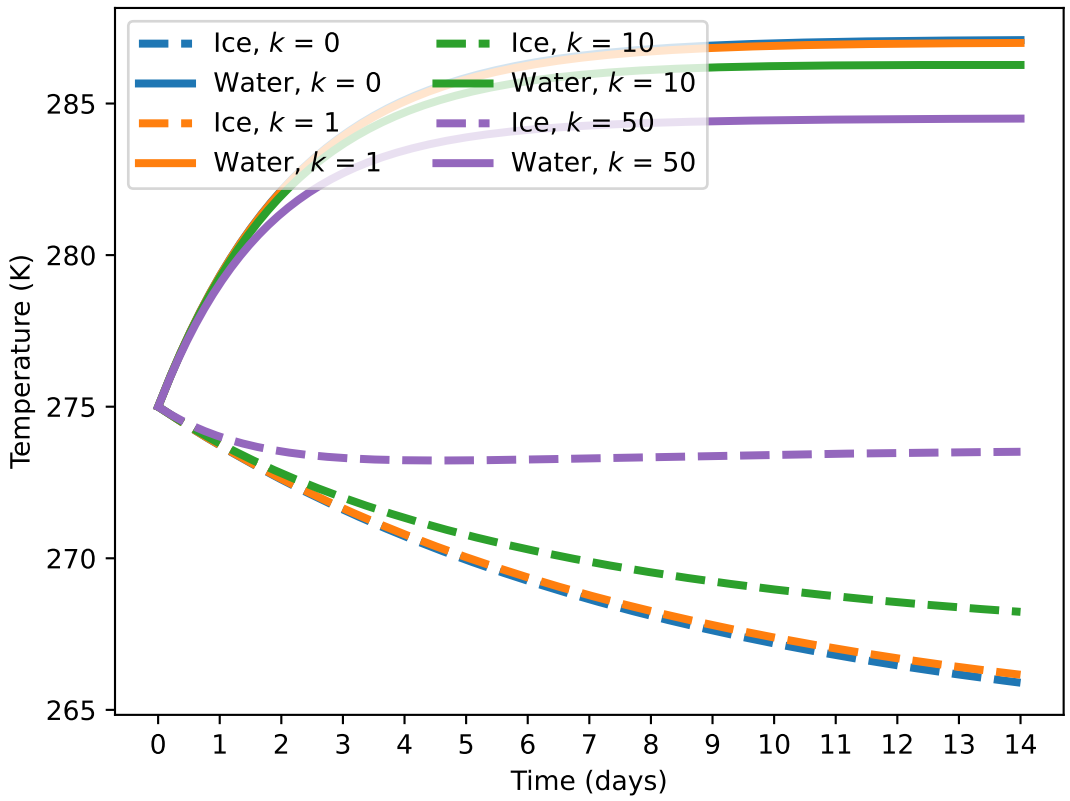


Figure 3.3: Temperature vs. time plot for parameter sweep for $k = 0, 1, 10, 50$. Open water is indicated by a solid line and ice-covered water is indicated by a dashed line.

Meanwhile, the difference in temperature between the ice-covered box and the open water is very large for all the values of k plotted in Figure 3.3, which indicates that the transport is very weak for these values. We can see this more clearly in Figure 3.4, where the temperature difference between the boxes is plotted for $k = 0, 1, 10, 50, 100$, and 500. The model was run for 21 days and initialized both boxes at $275K$ for consistency with

the results in Figure 3.3. In Figure 3.4, the temperature difference between adjacent open water and ice-covered water is greater than ten degrees for all k values shown in Figure 3.3. However, more values of the convective heat transfer coefficient are included in Figure 3.4, and the difference between the boxes for $k = 100$ and $k = 500$ show a smaller difference and therefore better mixing. It can be concluded that only for very large values of k can strong mixing be achieved.

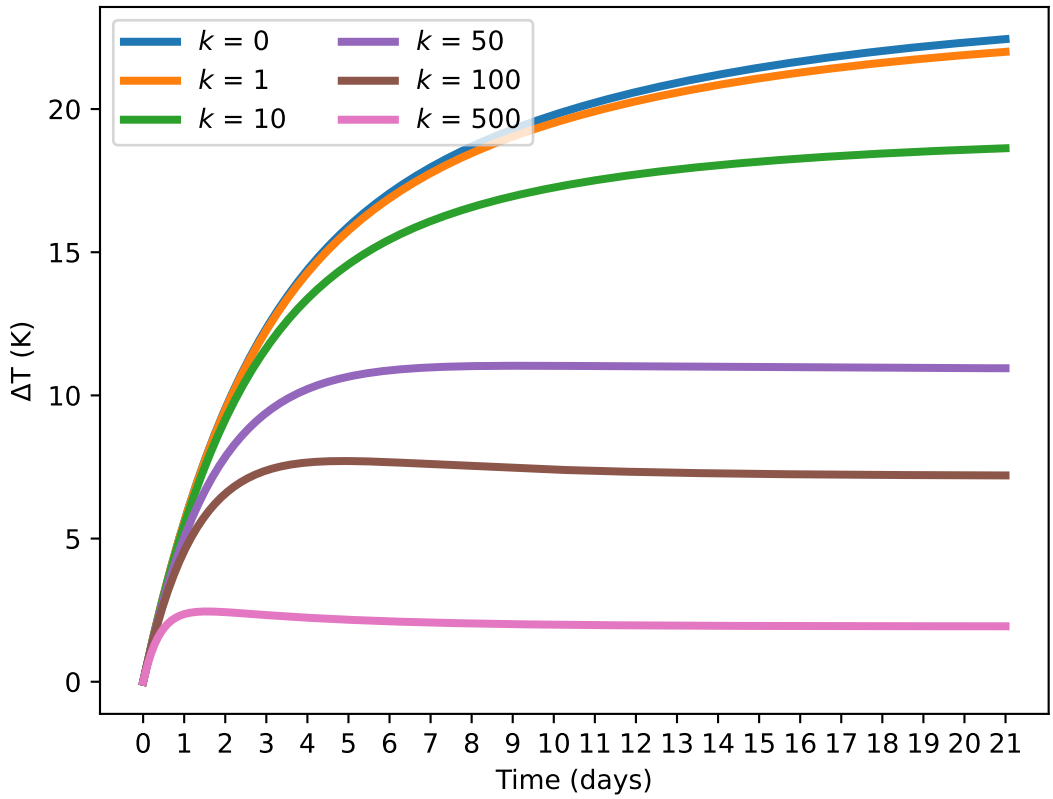


Figure 3.4: The temperature difference between boxes for $k = 0, 1, 10, 50, 100, 500$.

3.1.3 Nonlinear Transport

Now we will consider the model with only nonlinear transport. The governing equations for this model are:

$$\rho c_p V \frac{\mathrm{d}T_{ice}}{\mathrm{d}t} = (\frac{Q}{4}(1 - a_{ice}) - \epsilon_{ice}\sigma T_{ice}^4)LW - k_3(T_{ice} - T_{water})^3 WH \tag{3.5}$$

$$\rho c_p V \frac{\mathrm{d}T_{water}}{\mathrm{d}t} = (\frac{Q}{4}(1 - a_{water}) - \epsilon_{water}\sigma T_{water}^4)LW - k_3(T_{water} - T_{ice})^3 WH \tag{3.6}$$

Similarly to k, the convective heat transfer coefficient, k_3 is a convective heat transfer coefficient but for nonlinear heat transfer. It has units of $W/(m^2 \cdot K^3)$. Nonlinear heat transport is included to simulate stronger mixing between the boxes by cubing their temperature difference. While linear heat transport can be derived from Newton's law of cooling, our nonlinear heat transport does not have a direct equation that it can be traced back to.

Figure 3.5 shows the results of the model for $k_3 = 0, 1, 10$, and 50. The model was run for 14 days with initial conditions $T_{ice} = 275K$ and $T_{water} = 275K$. The steady-state temperatures for all the values of k_3 shown in Figure 3.5 are reasonable values that are not below freezing, except for the results related to $k_3 = 0$. The temperature differences between the respective values of k_3 show strong mixing for $k_3 = 10$ and $k_3 = 50$. Notably, the results for $k_3 = 0$ and $k_3 = 1$ show significant differences in steady-state temperature. This contrasts the results from Figure 3.3 where the results for $k = 0$ and $k = 1$ are nearly indistinguishable. This indicates that even a small amount of nonlinear transport can increase the mixing between boxes substantially.

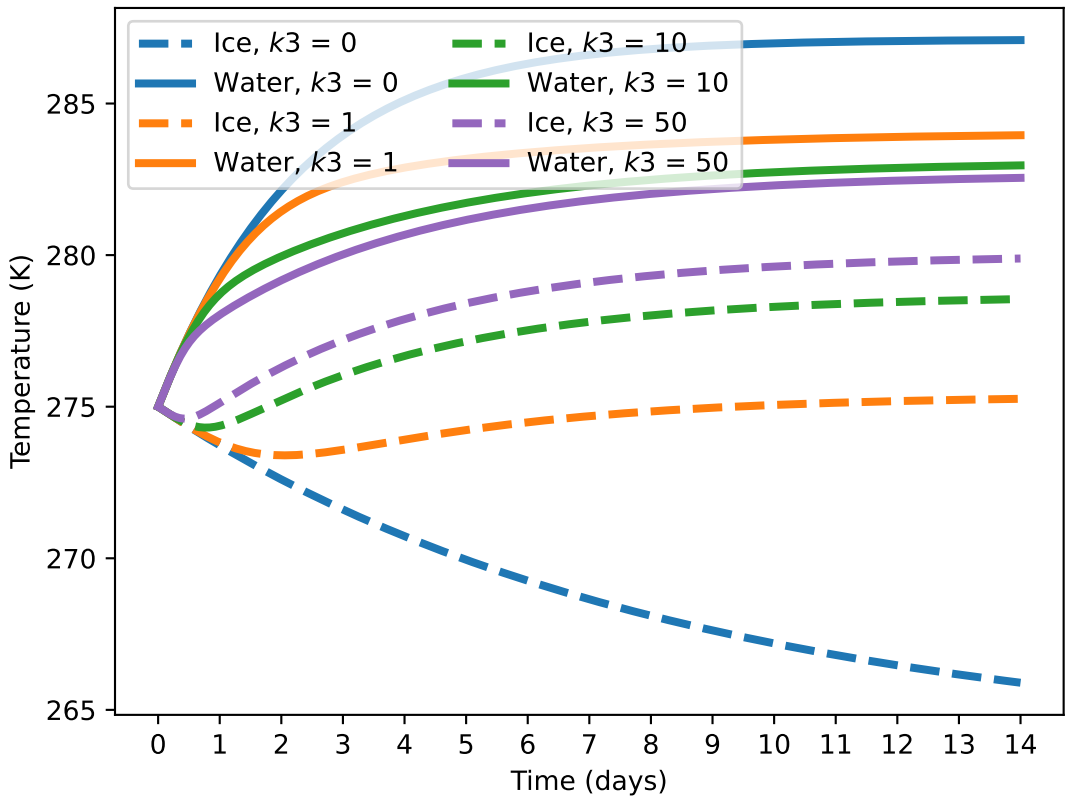


Figure 3.5: Temperature vs. time plot for parameter sweep for $k_3 = 0, 1, 10, 50$. Open water is indicated by a solid line and ice-covered water is indicated by a dashed line.

In Figure 3.6, we have the results of the temperature difference between the boxes for $k_3 = 0, 1, 10, 50, 100$, and 500. The model was run for 21 days with the same initial conditions as Figure 3.5. Here the difference between $k_3 = 0$ and $k_3 = 1$ is clearly shown. However, for the larger values of k_3, particularly $k_3 = 50$, 100, and 500, the influence of the nonlinear transport begins to wane as the steady-state temperature differences are all

close to each other.

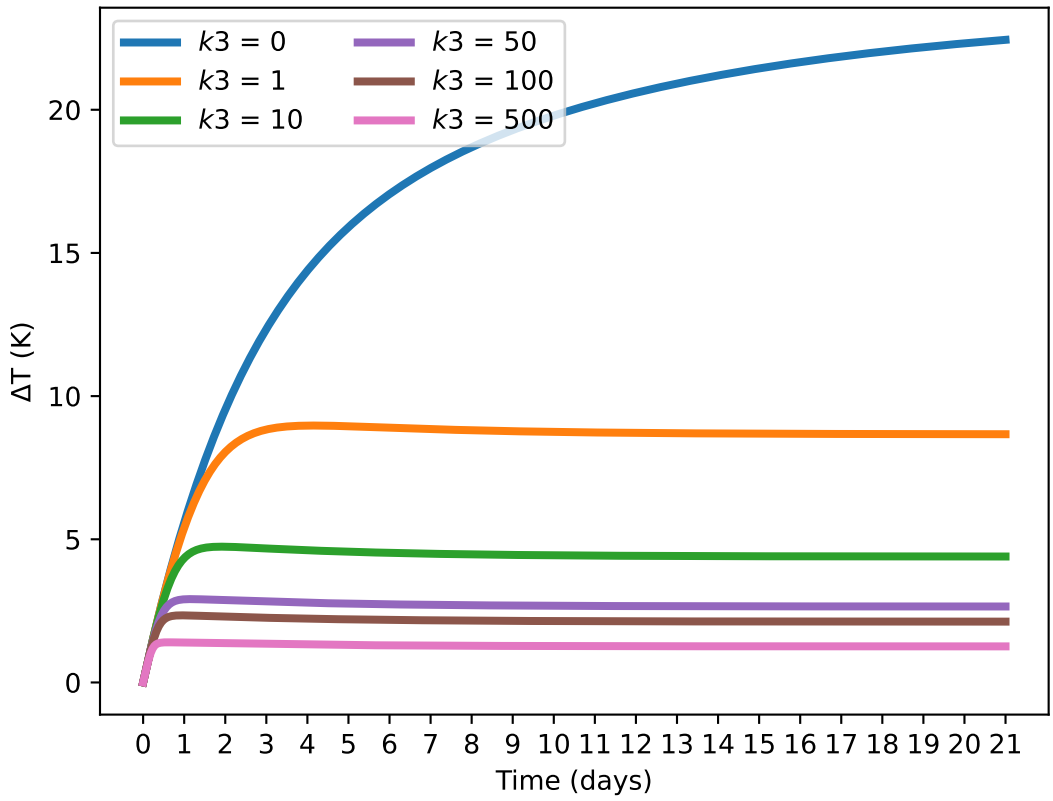


Figure 3.6: The temperature difference between boxes for $k_3 = 0, 1, 10, 50, 100, 500$.

3.1.4 Constant Insolation Framework Discussion

The results of the above sections show that a model with either linear or nonlinear transport can simulate strong mixing with the appropriate values of k and k_3. A model with nonlinear heat exchange can achieve significantly more mixing than a model with none at all with

very small values of k_3. Meanwhile, a model with linear heat exchange must have a very large k to simulate strong mixing and small values of k are similar to the model with no mixing at all. This might suggest that using only a nonlinear transport parameter is the best way to simulate strong mixing, however, the influence of the nonlinear transport plateaus at large values. This is likely because its cube power will decrease the magnitude of the term in the event that the temperature difference between the boxes is less than 1. So nonlinear transport will strongly mix boxes that have a large temperature difference, but when the ΔT of the two boxes is less than 1 it will only simulate weak heat exchange, if any at all. It is best to put a combination of linear and nonlinear transport in the model, so that strong mixing can be simulated without dependence on ΔT.

Another aspect that may affect the potential for strong mixing is the box dimensions. In Sections 3.1.1, 3.1.2, and 3.1.3, the dimensions of the box are $L_1 = L_2 = 1000m$. Meanwhile, the depth is $H = 20m$. These dimensions are visualized in Figure 3.7. They are not to scale.

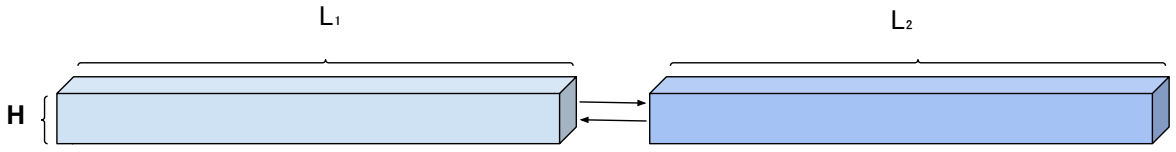


Figure 3.7: The dimensions of the boxes used to generate the results of the previous section.

Because the area over which the boxes are in contact is relatively small compared to the surface area of each box, it may be more difficult to simulate strong mixing in boxes with

the dimensions seen in Figure 3.7. In addition, it is difficult to determine what a reasonable temperature difference should be. Because the temperatures calculated are averages over the entire box, the more of each box that is not directly in contact with the other, the more reasonable a large difference in temperatures could be. In the case of the boxes like those shown in Figure 3.7, the far left edge of the first box is 2km away from the far right point of the second box and so it is possible that the exact temperatures in these areas could be very different from each other. The values of k and k_3 used for a pair of boxes that have greater depth would likely be much lower, since there would be more area over which convective heat transfer can occur.

3.2 Constant Insolation With Box Length Inequality

In the previous section, all results have been run for a pair of equal volume boxes. However, as the discussion of Section 3.1.4 suggests, box size plays a very important role in the behaviour of the system. Particularly, the length and height of the box can have significant impacts on the mixing potential and what is considered a realistic temperature difference at steady state. Here we will discuss the steady-state results of a constant insolation framework where the box sizes are unequal.

Recall from the dimensions shown in Figure 2.3 that the area over which the boxes are in contact with each other is $H * W$, and so the values of H and W for each box are by default equal to each other. The width, W, of the boxes already has no impact on the mixing between the boxes as it cancels out of both sides of Equations 2.17 and 2.18.

a_i	0.8
a_w	0.09
ϵ_i	0.25
ϵ_w	0.85
k	10
k_3	50
ρc_p	4.184e4

Table 3.1: Parameter set for Section 3.2

The height H is fixed at 20 meters for this section. Based on the results of Section 3.1 this section we will allow for nonlinear and linear transport, with $k = 10$ and $k_3 = 50$. The steady-state values of T_1 and T_2 are what will be analyzed in this section so we will allow the volumetric heat capacity to be $4.184 \times 10^4\ J/kg \cdot K$ so that the steady state is reached relatively quickly. The value of L is varied here, first with equal volume boxes as a benchmark and then with the ice length being half of the water length and then the reverse. A table of the parameter values for this section is below. The values used in this section are the same as in Section 3.1, save for the varied k and k_3.

Figure 3.8 is a benchmark result for the rest of this section. It has two boxes that have dimensions $L = 1000$, $H = 20$, and $W = 50$. The results show strong mixing between the two zones, which is to be expected with the chosen values of k and k_3. Notice that ΔT in Figure 3.8 is approximately 2.5 degrees. Figures 3.9 and 3.10 show the results for a box with a 1000m length ice box mixing with a 500m length water box and a 500m length ice

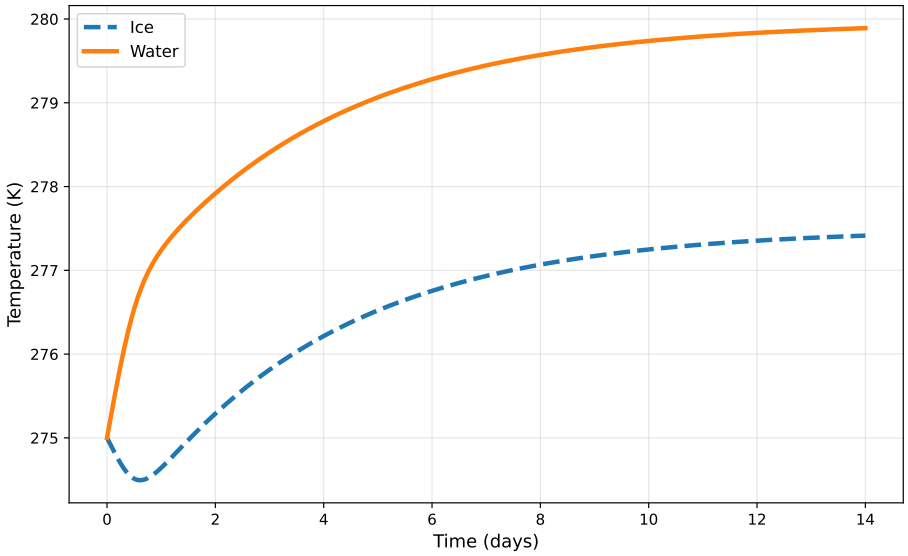


Figure 3.8: Plot of temperature vs time for equal length boxes.

box mixing with a 1000m length water box, respectively. In both figures, the temperature difference is approximately the same as in Figure 3.8. Each steady state settles with a ΔT of approximately 2.5 $^{\circ}C$. However, the average temperature overall is lower when the ice box is longer than when the water box is longer. When the ice box is longer, it settles at a steady-state temperature that is barely warmer than where it began and the steady-state temperature for the water box plateaus at a relatively low temperature. When the water box is longer, it appears to "give heat" to the ice covered box and both gain several degrees before settling at steady state. The steady-state temperatures of both boxes is relatively warm when the water box is larger, while the steady-state temperatures are comparatively cold when the ice-box is larger. However, the temperature difference between the boxes remains approximately the same regardless of box length.

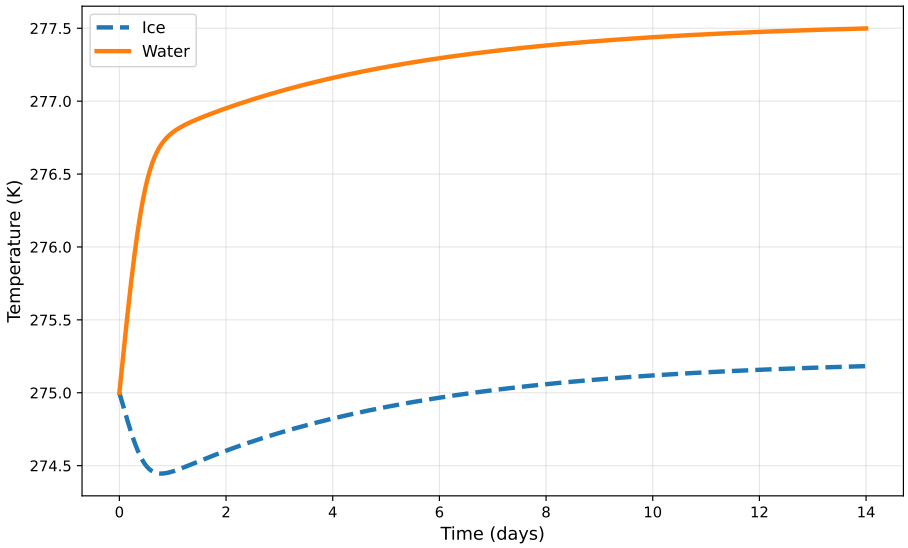


Figure 3.9: Plot of temperature vs. time for an open water box that has half the length of the ice covered box.

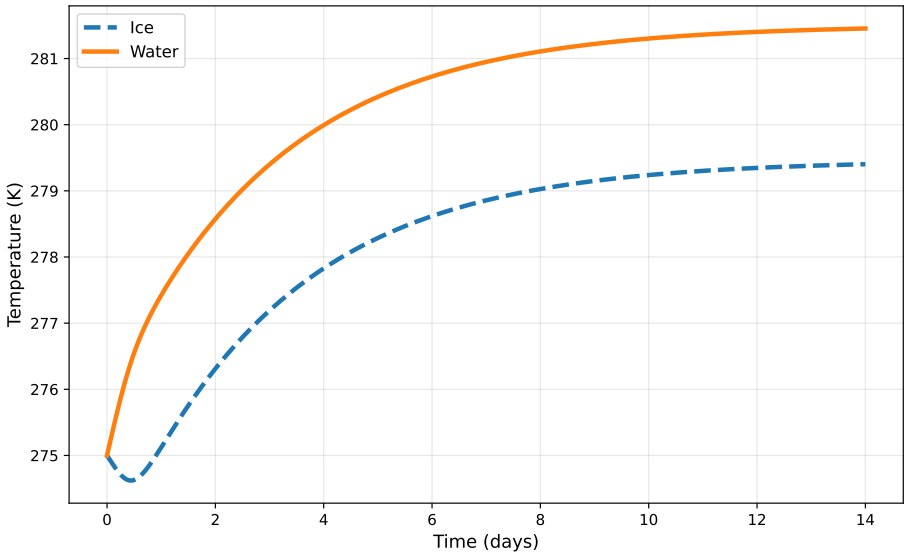


Figure 3.10: Plot of temperature vs. time for an ice covered box that has half the length of the open water box.

3.2.1 Unequal Box Length Discussion

The results of this section suggest that while an unequal box size has little effect on the steady-state temperature difference, it does affect the mean value of the temperature of both boxes. When the open water surface area is larger than the ice-covered surface area, the mean steady-state temperature is approximately $280.5K$, and when the reverse is true the mean steady-state temperature between the boxes is close to $276.5K$. This means that when ice is the dominant surface, the steady state temperature is lowered in both zones and when the open water prevails the steady state temperature for each area is raised.

3.3 Day-Night Cycle

The second section of results focuses on how the model performs under a day-night cycle. These conditions are more realistic for lakes across Canada and countries of similar latitude. As we are not focused on steady-state temperatures for this section, the heat capacity is set to its true value of $4.184 \times 10^6\ J/(kg \cdot K)$ and the density is set to $1000\ kg/m^3$. Rather, we want to see if the model can handle the changes in insolation without the temperatures of each becoming too cold. When night falls, the model loses its only external source of heat. So, it will rapidly lose heat, which could cause the temperatures to drop below freezing and continue. If both boxes have average temperatures below freezing, then there can no longer be convective heat transport between them, but more importantly this would not be characteristic of a real lake.

The day-night cycle is implemented by augmenting the insolation function. In Section

2.1.1, we define the incoming radiation from the Sun as

$$q_{in} = \frac{Q}{4}(1-a) \tag{3.7}$$

which is a constant in time. To implement the day–night cycle, we define a new function to describe the insolation, which is

$$q_{in} = \frac{Q}{4}(1-a) * (\lfloor \frac{t}{12} \rfloor \mod 2) \tag{3.8}$$

where t is in hours. This sets the insolation function to be equal to either 0 or $\frac{Q}{4}(1-a)$ every 12 hours and begins on a night. This cycle function is rudimentary. It does not take into account the Sun's cycle throughout the day, wherein there is maximal insolation around noon and less at dawn and dusk, and it does not account for the shorter days during the winter. However, it is enough to give us insight into how the model behaves when its heat source is cycled.

3.3.1 Day–Night Cycle Without Emissivity Switch

In this section, we will implement the day-night cycle function into the model as is. Figure 3.11 shows a plot of the results of the day–night cycle. The model was started with an initial temperature of $273.05K$ for each box and was run for 30 days. The blue zones on the plot indicate night and the white zones indicate day. The dimensions of both boxes are $L_1 = L_2 = 50m$, $W = 50m$, and $H = 100m$. These dimensions were chosen to allow for more mixing between the boxes and for a larger surface to absorb sunlight during the

day. The mixing parameters are set at $k = 10^4$ and $k_3 = 10^3$. However, given the very small temperature differences between the boxes, nonlinear transport has very little effect.

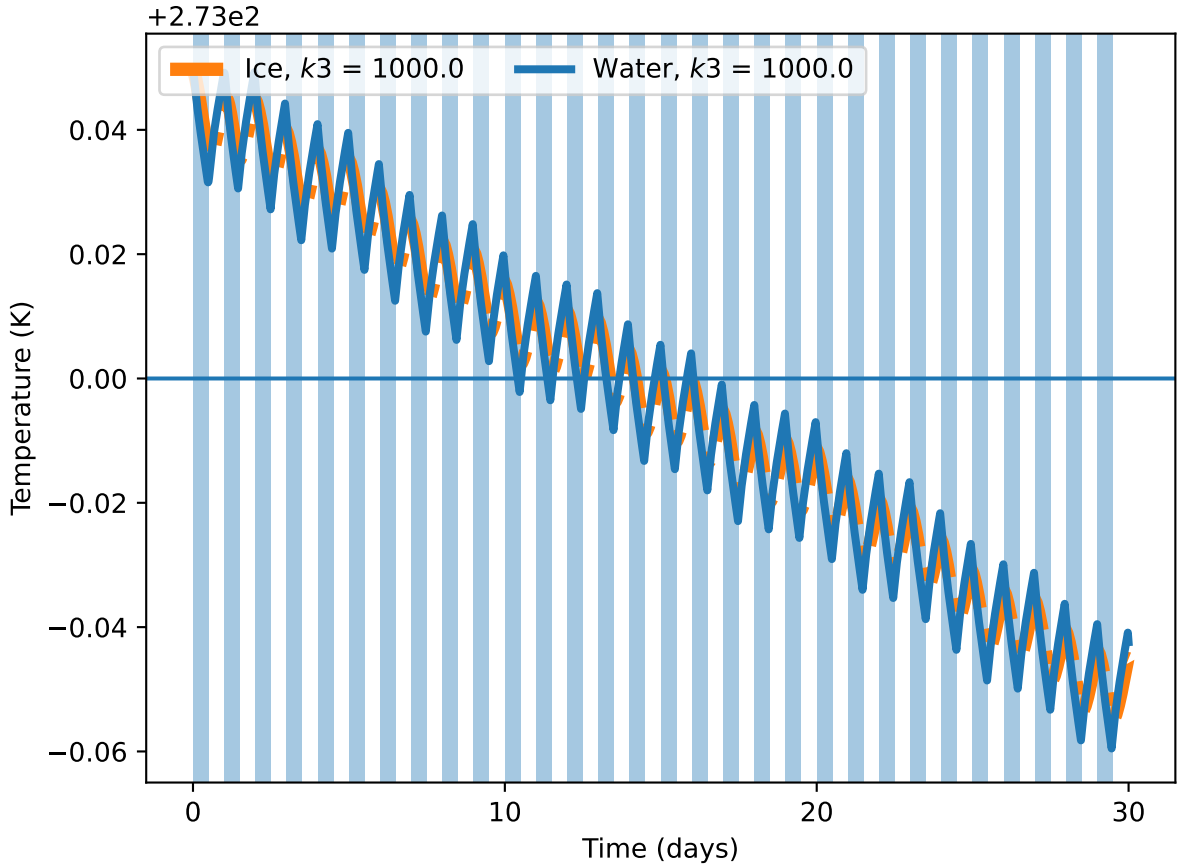


Figure 3.11: A plot of temperature vs. time for a day-night cycle where there is no emissivity switch. The vertical axis has a constant shift of $273K$.

Neither box gains much heat during the day due to water's high heat capacity. A small fraction of a degree is gained during the day, and only slightly more than that is lost overnight. However, it is enough that after approximately 2 weeks, temperatures drop

below freezing and continue to decrease. We know that our model ceases to make physical sense once the temperature of at least one box drops below the freezing level ($273K$), because convective heat transport can not occur between water and ice, or ice and ice. So we conclude that the model cannot provide reasonable results in a day-night cycle framework without modification.

3.3.2 Day–Night cycle With Emissivity Switch

The above results have shown that without changes, the model will not give physically relevant or reasonable results. The first modification we will try here is an emissivity "switch". When the temperature of the open water box drops below the freezing temperature, it is assumed to have become ice. Therefore, we change its emissivity from that of water, which is very high, to equal to the emissivity of ice, which is much lower. This will give the open-water box surface properties that reflect its state change. Figure 3.12 shows a diagram of the emissivity changing with temperature.

Figure 3.13 shows the results for the day-night cycle with the emissivity switch modification. The model had initial conditions $T_{ice} = 273.05K$ and $T_{water} = 273.05K$ and was run for 30 days. The mixing parameters are $k = 10^4$ and $k_3 = 10^3$, as before. With the addition of the emissivity switch, the temperatures no longer drop below freezing and continue. Instead, they settle into oscillations around $273K$, with nightly drops just below freezing before warming back up again.

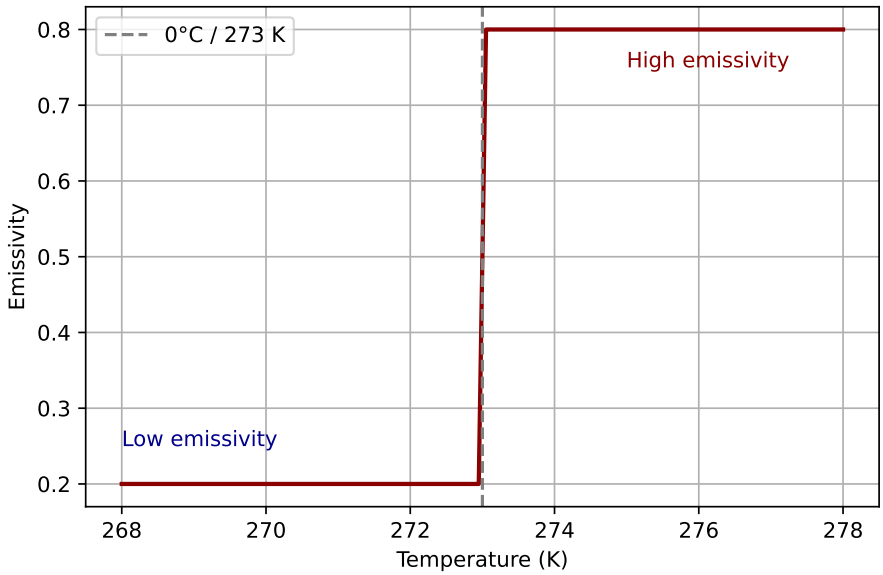


Figure 3.12: Diagram of the emissivity switching values with the temperature change.

3.3.3 Day-Night Cycle Discussion

With the implementation of the emissivity switch, the model is able to generate temperatures that are physically reasonable. This emissivity "switch" is a parameter that should be modified in accordance with the state change of the open water box, so in adding it the model has become more realistic. However, it should be noted that other parameters have also been modified to achieve the results shown in this section. The least realistic of these parameter modifications was to the intensity of the Sun, was increased by 50%. As well, the dimensions of the boxes were modified to be deeper and shorter, to increase mixing potential between the boxes. A deeper box will heat up more slowly, but will also shed heat more slowly, which could contribute to the very marginal temperature fluctuations

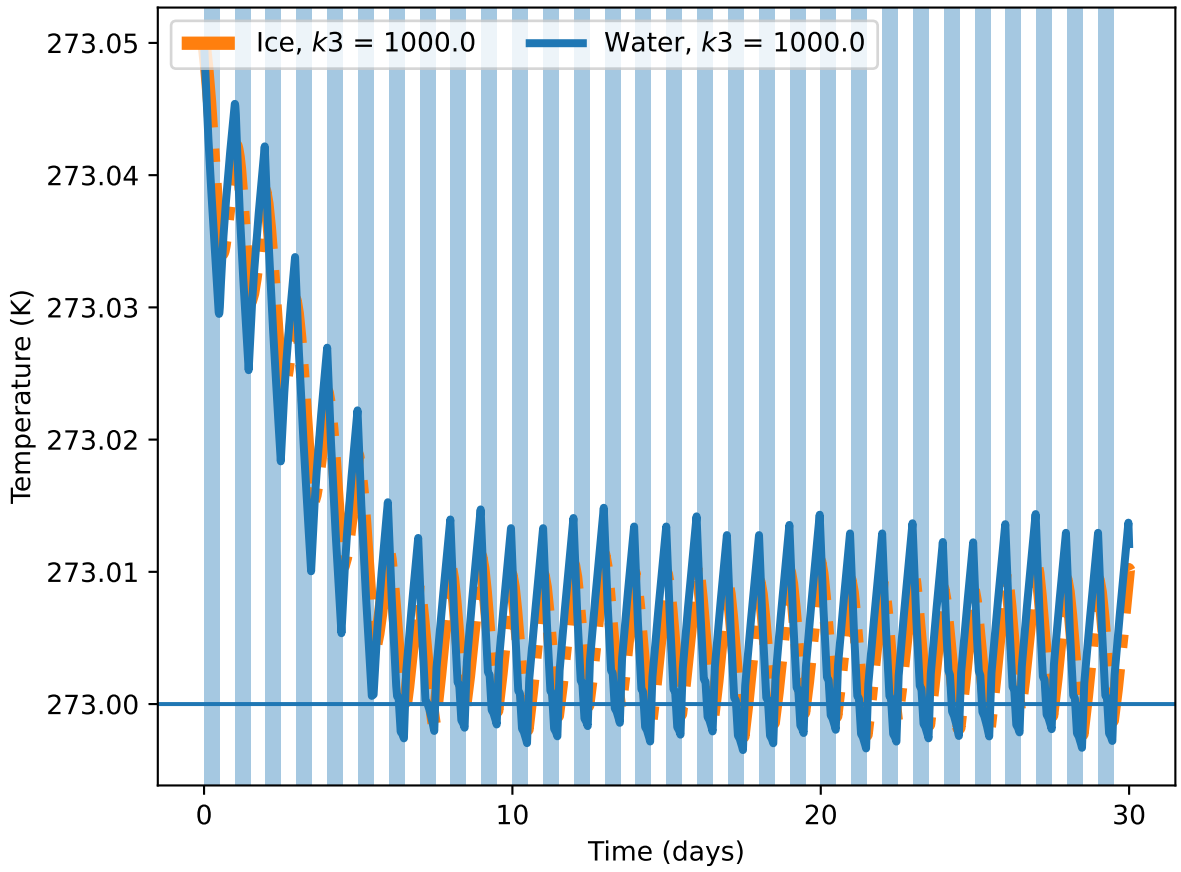


Figure 3.13: A plot of temperature vs. time for a day-night cycle where an emissivity "switch" is in place.

present in the results.

While the addition of the emissivity switch gives the model more realistic physics, it could be accompanied by an albedo switch which we have not implemented here. An albedo switch would change the albedo of the newly frozen open water box when it freezes, so that it will reflect more insolation. However, the albedo switch is not implemented here because it is assumed that the newly formed ice is not covered with snow, which is what gives older ice its high albedo. New, clear lake ice is not particularly reflective ([21]) and so an albedo switch has not been implemented.

These results build up from a rudimentary energy balance model with constant insolation and no mixing, to a day cycle model with an emissivity switch. Constant insolation models are a useful framework for setting parameters and examining steady-state values, but they cannot begin to simulate the cycle of actual lake temperatures. Then, without an emissivity switch the model again cannot properly simulate real life as even at temperatures that are technically frozen, the model still emits as though it is a black body even when it is not absorbing as one. The most complete and realistic model we have is the final model presented here, where a day cycle is implemented with an emissivity switch to represent the state change.

Chapter 4

Conclusions and Future Work

This thesis centers around the performance of a "simplest possible" box model for simulating the temperature of freshwater under partial ice cover. As most lake temperature models are not built for horizontal mixing between areas of ice cover and open water, the goal was to analyze the output of a model that is set up specifically with this behaviour in mind. To resolve the physics of inter-zone transport while still maintaining computational efficiency, we considered an energy budget box model with convective heat transport. In Chapter 2, we discuss the various terms of the differential equation: the incoming solar radiation, the emitted radiation, the linear heat transport, and the nonlinear heat transport. In Chapter 3 we then discuss the results of several quantitative experiments on the model. First, parameters are set by running constant insolation experiments, then complexity is built up by adding in a day–night cycle and then an emissivity switch. In section 3.1, the constant insolation experiments begin with boxes of equal size and first consider boxes with no transport between them. Then simulations are run with a range of values of both

the linear heat transport parameter, k, and the nonlinear heat transport parameter, k_3, to assess reasonable values for each. Still with constant insolation in section 3.2, boxes with different lengths are considered to assess the effect of box dimensions on the mixing and overall temperature. Then in section 3.3 we introduce a function for the insolation that approximates a day–night cycle, and then in this day-cycle framework we introduce an emissivity "switch" so that when the surface of the lake freezes the emissivity value changes to be that of ice rather than water.

The constant insolation experiments show that there may be a need for a nonlinear heat transport coefficient to bring the boxes to a reasonable temperature difference, depending on the true value of the convective heat transport parameter. In the day–night cycle framework, an equilibrium cycle is established when an emissivity switch is added for temperatures that dip below the freezing point of water. The day–night cycle model with emissivity switch represents the simplest possible model that still achieves realistic results. Overall, the model's ability to produce reasonable partial ice cover temperatures using the above–described simplest possible model appears from this work to be good, when nonlinear mixing and an emissivity switch are implemented.

For future work, the results of this thesis should be scaled up to four boxes that are all mixing with each other, as shown in the schematic in Figure 4.1. Adding more boxes to the model could increase the model's ability to simulate a body of water realistically. In a real lake, ice cover will certainly not cover exactly half of it but rather would cover the surface in a patch that would depend on the flow characteristics and bathymetry of the lake. Four boxes would allow for three distinct arrangements, shown in Figure 4.2.

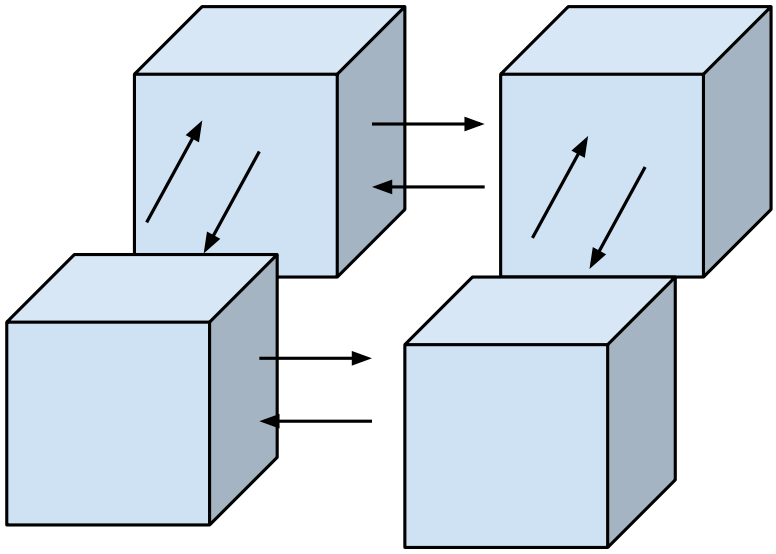


Figure 4.1: Schematic of transport between four boxes as would be seen in a four-box model.

Note that two ice-covered boxes (which is equivalent to two open water boxes) is only a meaningful configuration if the boxes are not side by side, as those results would effectively be a subset of the results shown in this thesis and not unique to the four-box model. For one ice covered box, results would do well to be compared directly with if possible, since such a configuration is the closest to what was used here.

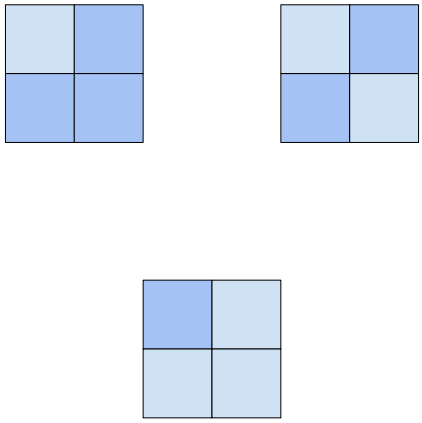


Figure 4.2: Relevant four-box model configurations for surface reflectivity. Other configurations, such as two side-by-side boxes with the same surface properties, would be a subset of the results shown in this thesis.

References

[1] Donovan Allum. *Simulations of Radiatively Driven Convection and Spatially Heterogeneous Solar Radiation Intensity in Ice-Covered Lakes*. Phd dissertation, University of Waterloo, Waterloo, ON, December 2023.

[2] Donovan JM Allum and Marek Stastna. Simulations of buoyant flows driven by variations in solar radiation beneath ice cover. *Physical Review Fluids*, 9(6):063501, 2024.

[3] Jay Austin and Steve Colman. A century of temperature variability in lake superior. *Limnology and Oceanography*, 53(6):2724–2730, 2008.

[4] Damien Bouffard and Alfred Wüest. Convection in lakes. *Annual Review of Fluid Mechanics*, 51(1):189–215, 2019.

[5] Laura C Brown and Claude R Duguay. The response and role of ice cover in lake-climate interactions. *Progress in physical geography*, 34(5):671–704, 2010.

[6] Great Lakes Commission. About the lakes. https://www.glc.org/lakes/. Accessed: 2025-08-08.

[7] Convection and conduction. https://www.ebsco.com/research-starters/science/convection-and-conduction. Accessed:2026-06-22.

[8] Claude R Duguay, Greg M Flato, Martin O Jeffries, Patrick Ménard, Kim Morris, and Wayne R Rouse. Ice-cover variability on shallow lakes at high latitudes: model simulations and observations. *Hydrological Processes*, 17(17):3465–3483, 2003.

[9] Claude R Duguay, Terry D Prowse, Barrie R Bonsal, Ross D Brown, Martin P Lacroix, and Patrick Ménard. Recent trends in canadian lake ice cover. *Hydrological Processes: An International Journal*, 20(4):781–801, 2006.

[10] Yu Ping Guan and Rui Xin Huang. Stommel's box model of thermohaline circulation revisited—the role of mechanical energy supporting mixing and the wind-driven gyration. *Journal of Physical Oceanography*, 38(4):909–917, 2008.

[11] Yukari Hori, Vincent YS Cheng, William A Gough, Jerry Y Jien, and Leonard JS Tsuji. Implications of projected climate change on winter road systems in ontario's far north, canada. *Climatic Change*, 148(1):109–122, 2018.

[12] Ravi K Jain, Jeremy K Domen, et al. *Environmental impact of mining and mineral processing: management, monitoring, and auditing strategies*. Elsevier, 2016.

[13] Stephen L Katz, Lyubov R Izmest'eva, Stephanie E Hampton, Ted Ozersky, Kirill Shchapov, Marianne V Moore, Svetlana V Shimaraeva, and Eugene A Silow. The "melosira years" of lake b aikal: Winter environmental conditions at ice onset predict under-ice algal blooms in spring. *Limnology and Oceanography*, 60(6):1950–1964, 2015.

[14] Thermohaline circulation - the stommel box model. https://www.pik-potsdam.de/members/willeit/klimageschichte-ubungen/stommel-model/tutorial.pdf. Accessed: 2026-06-26.

[15] NOAA-Great Lakes Environmental Research Laboratory. Great lakes ice cover. https://www.glerl.noaa.gov/data/ice/. Accessed: 2025-08-08.

[16] Matti Leppäranta. *Freezing of Lakes*, pages 11–50. Springer Berlin Heidelberg, Berlin, Heidelberg, 2015.

[17] Matti Leppäranta. Freezing of lakes. In *Freezing of Lakes and the Evolution of their Ice Cover*, pages 17–62. Springer, 2023.

[18] Gerrit Lohmann. Temperatures from energy balance models: The effective heat capacity matters. *Earth System Dynamics*, 11(4):1195–1208, 2020.

[19] John J Magnuson, Dale M Robertson, Barbara J Benson, Randolph H Wynne, David M Livingstone, Tadashi Arai, Raymond A Assel, Roger G Barry, Virginia Card, Esko Kuusisto, et al. Historical trends in lake and river ice cover in the northern hemisphere. *Science*, 289(5485):1743–1746, 2000.

[20] Frank Millerd. Global climate change and great lakes international shipping. *Wilfrid Laurier University, Waterloo, Ontario, Canada, May*, 2007.

[21] Maren Pauly Tristan Mills. Lake ice seasonality. https://ccin.ca/ccw/lakeice/overview/seasonality. Accessed: 2025-08-08.

[22] Dmitrii V Mironov. Parameterization of lakes in numerical weather prediction. Part 1: Description of a lake model. *German Weather Service, Offenbach am Main, Germany*, 2005.

[23] Abraham H Oort and JP Peixoto. *Physics of climate*. American Institute of Physics New York, 1992.

[24] Daniel Scott and University of Waterloo. Dept. of Geography. *The vulnerability of winter recreation to climate change in Ontario's Lakelands Tourism Region*. Department of Geography, University of Waterloo, 2002.

[25] Sapna Sharma, Kevin Blagrave, John J Magnuson, Catherine M O'Reilly, Samantha Oliver, Ryan D Batt, Madeline R Magee, Dietmar Straile, Gesa A Weyhenmeyer, Luke Winslow, et al. Widespread loss of lake ice around the northern hemisphere in a warming world. *Nature Climate Change*, 9(3):227–231, 2019.

[26] Henry Stommel. Thermohaline convection with two stable regimes of flow. *Tellus*, 13(2):224–230, 1961.

[27] Spectacular Northwest Territories. The north's cool highways. https://spectacularnwt.com/story/cool-highways-4-awesome-ice-roads-in-the-northwest-territories/. Accessed: 2025-08-08.

[28] MR Twiss, RML McKay, RA Bourbonniere, GS Bullerjahn, HJ Carrick, REH Smith, JG Winter, NA D'souza, PC Furey, AR Lashaway, et al. Diatoms abound in ice-

covered lake erie: An investigation of offshore winter limnology in lake erie over the period 2007 to 2010. *Journal of Great Lakes Research*, 38(1):18–30, 2012.

[29] Jia Wang, Xuezhi Bai, Haoguo Hu, Anne Clites, Marie Colton, and Brent Lofgren. Temporal and spatial variability of great lakes ice cover, 1973–2010. *Journal of Climate*, 25(4):1318–1329, 2012.

[30] Jiali Wang, Pengfei Xue, William Pringle, Zhao Yang, and Yun Qian. Impacts of lake surface temperature on the summer climate over the great lakes region. *Journal of Geophysical Research: Atmospheres*, 127(11):e2021JD036231, 2022.

[31] David M Wright, Derek J Posselt, and Allison L Steiner. Sensitivity of lake-effect snowfall to lake ice cover and temperature in the great lakes region. *Monthly Weather Review*, 141(2):670–689, 2013.

APPENDIX

Appendix A

Model Code

The main solver class is shown below:

```
import numpy as np
import matplotlib.pyplot as plt
from scipy.integrate import odeint
from dataclasses import dataclass
from scipy.integrate import solve_ivp



class TempSolver:
    """
```

```
Class that solves the coupled ODE to get temperatures of two boxes
with can have varying parameters between them.
"""

def __init__(self, a_i, a_w, Q, k, k3, e_i, e_water, cp,
             box_ice_size, box_water_size, daycycle=False, e_switch=False):

    # Albedos
    self.a_i = a_i
    self.a_w = a_w

    # Insolation terms
    self.Q = Q*1
    self.sun_energy_i = self.Q*(1 - self.a_i)/4
    self.sun_energy_w = self.Q*(1 - self.a_w)/4

    # SB constant
    self.sigma = 5.670374e-8

    # Transport parameters
    self.k = k
    self.k3 = k3
```

```
    # Emissivity values. e_water is set if the emissivity switch is off.
    self.e_i = e_i
    self.e_water = e_water

    # Rho (density in kg/m^3) and heat capacity
    self.cp = cp

    # Box size: (L,W,H)
    self.box_ice_size = box_ice_size
    self.box_water_size = box_water_size

    # Day cycle and emissivity switch. 'True' for ON and 'False' for OFF.
    If daycycle is OFF, then we have constant daylight and no nighttime.
    self.daycycle = daycycle
    self.e_switch = e_switch

def e_w(self,T):
    if T > 273:
        return 0.9
    else:
        return self.e_i

def thesun(self,t):
```

```
    energies = 1
    if self.daycycle:
        interval = 12*3600
        energies = (int(t)//interval)%2
        #print(f'time is {t/3600=} and energies is {energies}')
    return energies

def boxes(self,t,y):

    Ti, Tw = y

    emitted_energy_i = self.sigma*self.e_i

    # Emissivity switch = True if it is on
    if self.e_switch:
        emitted_energy_w = self.sigma*self.e_w(Tw)
        #print("emissivity switch is on")
    else:
        emitted_energy_w = self.sigma*self.e_water
    # print(f'k is {self.k}')
    # print(f'k3 is {self.k3}')
    dTidt = (self.thesun(t)*self.sun_energy_i
    - emitted_energy_i*Ti**4)/
```

```
        (self.cp*self.box_ice_size[2])
        - (self.k*(Ti - Tw) + self.k3*(Ti - Tw)**3)/(self.cp*self.box_ice_size[0])

        dTwdt = (self.thesun(t)*self.sun_energy_w -
        emitted_energy_w*Tw**4)/(self.cp*self.box_water_size[2])
        - (self.k*(Tw - Ti) + self.k3*(Tw - Ti)**3)/(self.cp*self.box_water_size[0])
        return [dTidt, dTwdt]

    def get_sol(self,y0,start_time,end_time,num_points):

        solutions = solve_ivp(self.boxes, [start_time, end_time], y0,
        method='LSODA',dense_output='True', max_step = 5000)
        t = np.linspace(start_time, end_time, num_points)
        return solutions.sol(t)
```

Plotting functions are in the linked Github repository: https://github.com/erikakem/ThesisProject